Biophysical *Journal*
Article

Biophysical Society

^{2}H-NMR and MD Simulations Reveal Membrane-Bound Conformation of Magainin 2 and Its Synergy with PGLa

Erik Strandberg,[1] Diana Horn,[2] Sabine Reißer,[1,3] Jonathan Zerweck,[2] Parvesh Wadhwani,[1] and Anne S. Ulrich[1,2,*]
[1]Institute of Biological Interfaces (IBG-2), [2]Institute of Organic Chemistry, and [3]Institute of Physical Chemistry, Karlsruhe Institute of Technology, Karlsruhe, Germany

ABSTRACT Magainin 2 (MAG2) and PGLa are two α-helical antimicrobial peptides found in the skin of the African frog *Xenopus laevis*. They act by permeabilizing bacterial membranes and exhibit an exemplary synergism. Here, we determined the detailed molecular alignment and dynamical behavior of MAG2 in oriented lipid bilayers by using ^{2}H-NMR on Ala-d_3-labeled peptides, which yielded orientation-dependent quadrupolar splittings of the labels. The amphiphilic MAG2 helix was found to lie flat on the membrane surface in 1,2-dimyristoyl-*sn*-glycero-3-phosphatidylcholine (DMPC)/1,2-dimyristoyl-*sn*-glycero-3-phosphatidylglycerol (DMPG) and 1-palmitoyl-2-oleoyl-*sn*-glycero-3-phosphatidylcholine (POPC)/1-palmitoyl-2-oleoyl-*sn*-glycero-3-phosphatidylglycerol (POPG), as expected, with a tilt angle close to 90°. This orientation fits well with all-atom molecular-dynamics simulations of MAG2 performed in DMPC and DMPC/DMPG. In the presence of an equimolar amount of PGLa, the NMR analysis showed that MAG2 becames tilted at an angle of 120°, and its azimuthal rotation angle also changes. Since this interaction was found to occur in a concentration range where the peptides per se do not interact with their own type, we propose that MAG2 forms a stable heterodimer with PGLa. Given that the PGLa molecules in the complex are known to be flipped into a fully upright orientation, with a helix tilt close to 180°, they must make up the actual transmembrane pore. We thus suggest that the two negative charges on the C-terminus of the obliquely tilted MAG2 peptides neutralize some of the cationic groups on the upright PGLa helices. This would stabilize the assembly of PGLa into a toroidal pore with an overall reduced charge density, which could explain the mechanism of synergy.

INTRODUCTION

Antimicrobial peptides (AMPs) are found in most types of organisms and constitute an innate protection against microorganisms (1–3). In many cases, the mechanism of the antimicrobial activity of AMPs is attributed to the permeabilization of bacterial membranes (4–6). Some AMPs show synergistic effects, such that the activity of a mixture of two peptides is substantially higher than the sum of the activities of the individual agents (7,8), which makes them even more interesting to study.

Magainin 2 (MAG2; sequence GIGKFLHSAKKFGKAF VGEIMNS) was extracted from the skin of the African frog *Xenopus laevis* and found to exhibit modest antimicrobial activity (9). MAG2 forms an amphiphilic α-helix when bound to a lipid bilayer and has been proposed to kill bacteria by forming toroidal wormhole pores in their membranes (6,10–15). It is part of the larger magainin family of AMPs from the same frog, which has been proposed to share a common gene ancestry (16,17). One of these peptides, PGLa (sequence GMASKAGAIAGKIAKVALKAL-NH_2), exhibits a strong synergistic antimicrobial activity together with MAG2 (18–22). Reports showing that the strongest synergy is found for 1:1 mixtures of the two peptides suggest that they might form heterodimers, which would be responsible for the synergy (21). According to a cross-linking study in membranes, such heterodimers are most likely arranged in parallel, with the most efficient linkage connecting the two C-termini (23).

Solid-state NMR on isotope-labeled peptides is a convenient method to determine the orientation of membrane-active peptides in macroscopically aligned lipid bilayers under quasi-native conditions (24–27). With a single ^{15}N label, an approximate tilt angle of the peptide can be determined from a simple one-dimensional (1D) experiment, but the use of fully ^{15}N-labeled peptides and two-dimensional (2D)-NMR can provide a more accurate tilt angle. With

Submitted March 23, 2016, and accepted for publication October 6, 2016.
*Correspondence: anne.ulrich@kit.edu
Editor: Francesca Marassi.
http://dx.doi.org/10.1016/j.bpj.2016.10.012

additional information from specifically labeled peptides, it is also possible to determine the azimuthal rotation angle, which describes the orientation of side chains with respect to the membrane and is defined as a rotation around the peptide's long axis. Alternatively, ^{2}H- and ^{19}F-NMR on analogs carrying selective labels in the side chains can be used to obtain accurate tilt and azimuthal angles simultaneously.

The orientation of PGLa and MAG2 has been studied in membranes using solid-state ^{15}N-NMR on ^{15}N-labeled peptides. In unsaturated lipids such as 1-palmitoyl-2-oleoyl-*sn*-glycero-3-phosphatidylcholine (POPC) and 1-palmitoyl-2-oleoyl-*sn*-glycero-3-phosphatidylethanolamine (POPE)/1-palmitoyl-2-oleoyl-*sn*-glycero-3-phosphatidylglycerol (POPG), even at high peptide/lipid molar ratios (P/L), both peptides lie flat on the membrane surface, alone as well as in a 1:1 mixture (26,28–36). In saturated lipids such as 1,2-dimyristoyl-*sn*-glycero-3-phosphatidylcholine (DMPC)/1,2-dimyristoyl-*sn*-glycero-3-phosphatidylglycerol (DMPG), a different behavior is found: on its own, PGLa lies flat on the membrane surface at low P/L, and it becomes obliquely tilted at P/L = 1:100 and higher concentrations. In a 1:1 mixture with MAG2, PGLa flips into the membrane in an upright transmembrane orientation that is compatible with the formation of a membrane-spanning toroidal pore. MAG2, on the other hand, lies flat on the membrane in DMPC/DMPG up to P/L = 1:30, becomes obliquely tilted at 1:10, and assumes only a slight tilt when PGLa is present. No inserted orientation has been found using solid-state NMR (26,28,29).

PGLa has also been studied using ^{2}H- and ^{19}F-NMR, and it was found that PGLa can change between two distinct states: at low concentrations in DMPC/DMPG a surface-bound S-state is found in which the helix axis is almost parallel to the membrane surface, and at higher concentrations a more tilted T-state is found in which the angle between the bilayer surface and the helix is close to 35° (37–40). In a mixture with MAG2, an inserted I-state is found with an almost upright (transmembrane) orientation of the peptide that is compatible with the formation of a membrane-spanning pore (20,41). The S-, T-, and I-states can also be observed within one sample by varying the temperature through the lipid phase transition and beyond (42). The S- and T-states of PGLa have also been investigated using molecular-dynamics (MD) simulations (43,44).

So far, the alignment of MAG2 has only been studied by ^{15}N-NMR, but here we present a study of Ala-d_3-labeled MAG2 using solid-state ^{2}H-NMR and MD simulations. Many MD studies have examined AMPs in membranes, but no long all-atom simulation of MAG2 has been published yet. Simulations also need to be validated by high-resolution experimental data, which have not previously been available for MAG2. A refined picture of this peptide in the membrane can thus be obtained from the combined NMR and MD results presented here. Basically, we find that MAG2 is oriented almost completely flat on the membrane surface in both POPC/POPG and DMPC/DMPG, and no significant change in orientation is seen as a function of peptide concentration in DMPC/DMPG. There is a change in the orientation of MAG2 in the presence of PGLa, but in contrast to PGLa, MAG2 does not insert into the membrane in a transmembrane orientation, and tilts by only ~30°. From these findings, the first, to our knowledge, model for the synergistic interaction of MAG2 with PGLa can be derived.

MATERIALS AND METHODS

For details regarding the materials and methods used in this work, see Supporting Materials and Methods in the Supporting Material.

RESULTS AND DISCUSSION

A total of 10 different Ala-d_3 substituted MAG2 analogs (listed in Table S1) were successfully synthesized and purified. We previously showed that all of these peptides are unstructured in aqueous buffer but form an α-helix in the presence of DMPC/DMPG (3:1) lipid vesicles (45). We also found that all of these analogs have an antimicrobial activity with a minimum inhibitory concentration (MIC) comparable to that of the MAG2 wild-type (MAG2-WT) (45), with certain exceptions that will be discussed below. We may therefore assume that the analogs have the same structure as the WT peptide and can be used to determine the structure and orientation of MAG2 in membranes.

^{2}H-NMR experiments were performed on peptide-lipid samples that were macroscopically oriented on thin glass plates, with their bilayer normal aligned parallel to the external magnetic field. To allow a comparison with previous ^{15}N-NMR experiments, several different lipid systems were used. For each sample, ^{31}P-NMR spectra were recorded before and after the ^{2}H-NMR experiment to check the sample quality, and in particular to confirm that the sample was well oriented and that the lipids were in the lamellar liquid crystalline phase (data not shown). In the ^{2}H-NMR spectrum, the CD_3 group of an Ala-d_3 label gives a quadrupole splitting that depends on the orientation of the C_α-CD_3 bond relative to the magnetic field. This splitting $\Delta\nu_q$ reflects the orientation of the labeled peptide side chain in the magnetic field, such that in our oriented samples the collection of all $\Delta\nu_q$ can be used to determine the orientation of the entire peptide helix with respect to the membrane normal.

In POPC/POPG (9:1), all samples give well-resolved spectra at a P/L of 1:50 (see Fig. 1 *A*) and a distinct splitting arises from the oriented peptides (listed in Table 1). The central peak at 0 ppm is due to residual ^{2}H in the water, as shown in Fig. 1 *C*, which shows one spectrum from a lipid sample (DMPC/DMPG 3:1) without peptide. The central peak may also contain some contribution from unbound peptides, but in anionic PG-containing bilayers, a positively

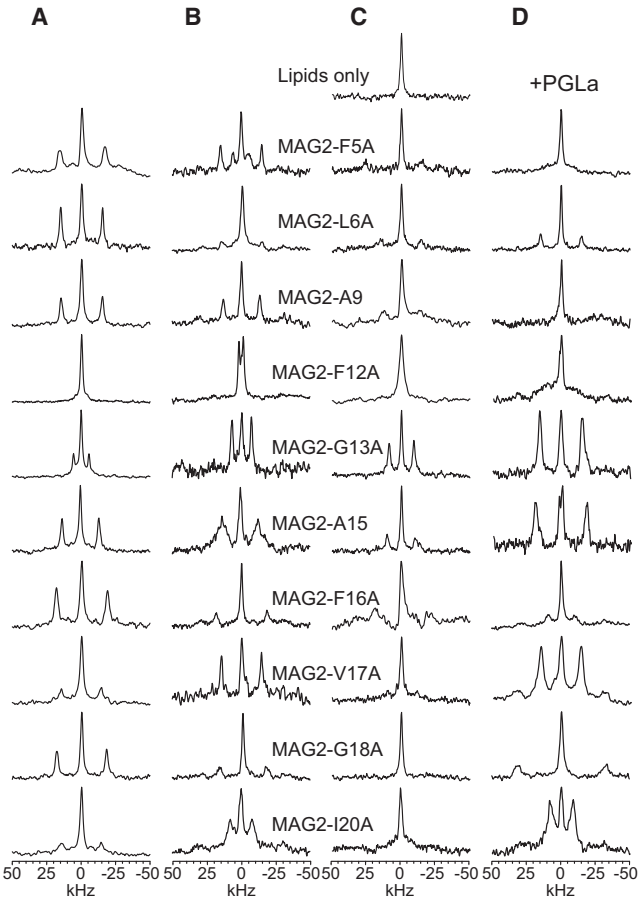

FIGURE 1 ^{2}H-NMR spectra of the Ala-d_3-labeled MAG2 analogs. Each row contains the spectra from one selectively labeled position, as indicated by the peptide name. (*A–D*) In each column, a different lipid system was used: (*A*) MAG2/POPC/POPG (2:90:10), (*B*) MAG2/DMPC/DMPG (1:75:25), (*C*) MAG2/DMPC/DMPG (2:75:25), and (*D*) PGLa/MAG2/DMPC/DMPG (1:1:75:25).

charged peptide like MAG2 is expected to bind electrostatically to the membranes, and hence such a contribution would probably be small (39). Only in the case of MAG2-F12A is no distinct splitting seen, but this is most likely attributed to a splitting of 0 kHz, which would mean that the C_α-CD_3 bond is oriented close to the magic angle. In a few cases, a second signal with a low intensity showing another splitting is observed, as discussed in Supporting Material (see Figs. S3 and S4 for more detailed spectra). We also prepared two samples (MAG2-F16A and MAG2-V17A) in POPC/POPG (9:1) at P/L = 1:100 and obtained almost the same splittings. This finding indicates, as expected, that the peptide orientation did not change between these peptide concentrations; hence, we did not carry out the full set of experiments at lower peptide concentrations.

With the full set of quadrupole splittings available, we performed a fit to determine the helix orientation in the membrane. The orientation can be defined by the tilt angle τ and the azimuthal angle ρ, as illustrated in Fig. S1. The fit results from the ^{2}H-NMR data of POPC/POPG samples are given in Fig. 2. When all 10 data points are used, a poor fit is found with a root mean-square deviation (RMSD) of 5.0 kHz. However, it is evident from the quadrupolar wave curves that the value of $\Delta\nu_q$ from position Ile-20 does not fit to the other data points. When this data point is excluded, a much better fit is found with an RMSD of 2.8 kHz (see Fig. 2 *C*). The resulting helix orientation is almost identical for these two fits, as shown in Table 2. The peptide tilt angle τ is 91° and its azimuthal rotation angle ρ is 174° in the fit without position Ile-20 (see Fig. 2 *A*), differing only by 1–3° from the fit including position Ile-20. We thus conclude that the splitting from position Ile-20, which is close to the C-terminus of the peptide, does not fit to our assumed ideal α-helix, because the C-terminus of MAG2 may be somewhat unraveled. It would not be unexpected to find that this anionic region with two negative charges (Glu-19 and the free C-terminus) is less stable in an anionic bilayer than the cationic N-terminal and central parts of the peptide.

A tilt angle close to 90° corresponds to a peptide lying flat on the membrane surface, as expected for an amphiphilic helix. This orientation was previously proposed for MAG2 in POPC/POPG from 1D ^{15}N-NMR experiments (28,29,46) and was confirmed here with higher accuracy. The azimuthal angle ρ (rotation around the helix axis) was not available from the 1D ^{15}N-NMR data, but a comprehensive 2D NMR analysis of fully ^{15}N-labeled MAG2 gave the full orientation of the peptide in POPC/POPG (4:1) at P/L = 1.6:100 (36). Values of τ and ρ are not explicitly stated in this work but can be estimated from the corresponding figure to be τ = ~90° and ρ = ~165° (using our definition). This fits well with our result (ρ = 174°) and describes a peptide orientation in which the polar sector (see Figs. S6 and S7) is pointing out of the membrane into the aqueous phase, as expected from biophysical considerations. We note that a similar overall peptide orientation was reported for the related amphipathic α-helical peptide MSI-103 in all tested lipid systems containing unsaturated lipids (47). We thus propose that this flat, surface-bound orientation is generally characteristic for amphipathic α-helical peptides in lipids with a negative spontaneous curvature (28,47,48). The four-parameter fitting procedure also revealed some information about the dynamical behavior of MAG2 in the membrane-bound state, namely, the degree of whole-body fluctuations around τ and ρ (see Fig. 2 *B*). They are described here by the width of the distributions σ_τ and σ_ρ, which show a very small variation of the tilt angle and a larger variation of the rotation angle (~15°). The same kind of dynamics was reported for MSI-103 in lipids with a negative spontaneous curvature (47).

In DMPC/DMPG (3:1), well-resolved spectra were found for all labels at a low peptide concentration, i.e., at P/L = 1:100 (see Fig. 1 *B*), and the splittings were similar to those found in POPC/POPG (see Table 1). More details about the

TABLE 1 Experimentally Determined or MD Derived ^{2}H-NMR Quadrupolar Splittings of MAG2 in Different Lipid Systems

	Quadrupolar Coupling (kHz)					
Lipid	POPC/ POPG	DMPC/ DMPG	DMPC/ DMPG	DMPC/DMPG + PGLa	DMPC (MD)	DMPC/DMPG (MD)
P:L	2:90:10	1:75:25	2:75:25	1:1:75:25	1:128	1:96:32
MAG2-F5A	(+)33.0	(+)30.0	not clear	not clear	+24.9	+7.9
MAG2-L6A	(−)30.4	(−)29.5	(−)28.8	(−)29.8	−30.8	−35.2
MAG2-A9	(+)30.2	(+)27.0	(+)25.9	not clear	+29.4	+8.7
MAG2-F12A	0	(+)3.2	0	not clear	+9.7	−7.0
MAG2-G13A	(−)11.3	(−)14.0	(−)18.1	(−)29.8	−26.2	−33.0
MAG2-A15	(−)26.7	(−)26.2	(−)20.9	(+)25.3	−26.0	−28.6
MAG2-F16A	(+)37.1[a]	(+)36.7	(+)37.2	(−)19.3	+33.5	+25.6
MAG2-V17A	(−)29.1[b]	(−)29.0	(−)29.9	(−)31.7	*+22.6*	*−31.8*
MAG2-G18A	(+)36.0	(+)34.3	not clear	+64.8	*−17.6*	*−7.9*
MAG2-I20A	(+)28.5	(+)15.8	(+)13.5	(−)16.3	*+38.6*	*+50.5*

NMR data were collected using macroscopically oriented samples, set with the membrane normal parallel to the magnetic field. The splitting obtained from a ^{2}H-NMR experiment is an absolute value, but its sign can be deduced from the fitting curve and is given in parentheses. Splittings from the MD trajectory are calculated with the sign, and in this case the sign is given without parentheses. In the MD simulations, the peptide is not helical from position 17 onward (marked in italics).

[a]A 1:90:10 sample gave 36.0 kHz.

[b]A 1:90:10 sample gave 28.9 kHz.

determination of splittings are given in Supporting Material. MAG2-F5A also gave a smaller splitting (half that of the main splitting), which is most likely due to some of the peptides being in unoriented membranes (39,40). MAG2-F12A showed a resolved splitting of only 3 kHz, supporting our interpretation that the splitting in POPC/POPG of this position was close to zero. The main difference is seen for MAG2-I20A, where a much smaller splitting was found in DMPC/DMPG. When we fitted these data (Fig. 3, *A–C*), we obtained a good fit using all 10 data points, with the same peptide orientation and dynamics as observed in POPC/POPG ($\tau = 91°$, $\rho = 174°$). In this case, $\Delta\nu_q$ from position Ile-20 does fit with the rest of the data points, suggesting that the α-helix may be more well-defined toward the C-terminus in DMPC/DMPG (3:1) compared with POPC/POPG (9:1).

For other related peptides from the magainin family, such as MSI-103 (47) and PGLa (37–40,49), an essentially flat surface-bound state was also found in DMPC or DMPC/DMPG at low peptide concentrations. However, at a higher P/L of 1:50, those peptides were found to be tilted into the membrane (28,29,37–40,45,50). Therefore, we also checked MAG2 at P/L = 1:50 in DMPC/DMPG (3:1). In this case, the spectral quality was worse (see Fig. 1 *C*) and splittings were harder to determine. More details about the determination of splittings from these spectra are given in Supporting Material. We prepared several duplicate samples of the problematic labeled positions and tried different sample preparation methods (see Supporting Materials and Methods), but in some cases it was not possible to resolve the quadrupole splitting. Such problems might be due to peptide aggregation, a loss of sample alignment, or unfavorable NMR relaxation behavior. Especially for MAG2-F5A, MAG2-F12A, and MAG2-G18A, we observed only a central peak, and no clear splitting. For most of the other positions, however, the splittings did not change much compared

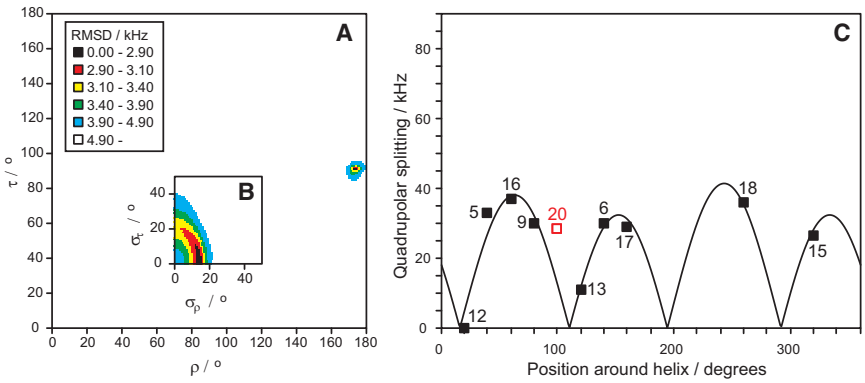

FIGURE 2 Best-fit analysis of the ^{2}H-NMR splittings from MAG2 in POPC/POPG (90:10) at P/L = 1:50. (*A*) RMSD plot of the fit as a function of peptide orientation in terms of the helix tilt and rotation angles τ and ρ. RMSD values for each τ-ρ combination are indicated by a color code. There is only a single well-defined minimum at $\tau = 91°$ and $\rho = 174°$. (*B*) RMSD plot as a function of the corresponding dynamical parameters, i.e., of the fluctuation deviations σ_τ and σ_ρ (same color code as in *A*). (*C*) The helical wave plot shows the curve of the splittings calculated from the best-fit parameters, together with the experimental data points. Residues are shown projected around the helical axis according to the helical wheel (see Fig. S6). Residue numbers are given next to the data points. Data from the most C-terminal position 20 was not used in the fit (*unfilled symbol*). To see this figure in color, go online.

TABLE 2 Best-Fit Orientations of MAG2 in Lipid Bilayers from ^{2}H-NMR Data and from Splittings Back-Calculated from the MD Trajectory

Lipid System	P/L	Positions Used in the Fit	τ (°)	ρ (°)	σ_τ (°)	σ_ρ (°)	RMSD (kHz)
^{2}H-NMR							
POPC/POPG	2:90:10	10 (all)	90	171	1	13	5.0
POPC/POPG	2:90:10	9 (not 20)	91	174	0	14	2.8
DMPC/DMPG	1:75:25	10 (all)	91	174	1	16	2.4
DMPC/DMPG +PGLa	2:75:25	8 (not 5,18)	94	174	0	14	3.1
DMPC/DMPG	1:1:75:25	7 (not 5,9,12)	122	147	0	18	3.0
MD							
DMPC	1:128	1–23	51	144	12	42	9.3
DMPC	1:128	1–17	91	174	0	14	8.7
DMPC	1:128	3–17	93	177	1	15	4.0
DMPC	1:128	3–16	94	176	14	8	3.7
DMPC	1:128	4–16	94	176	18	5	3.8
DMPC	1:128	3–15	93	176	5	12	3.9
DMPC/DMPG	1:96:32	1–23	65	3	29	0	13.5
DMPC/DMPG	1:96:32	1–17	105	179	4	0	5.6
DMPC/DMPG	1:96:32	3–17	104	177	0	0	3.1
DMPC/DMPG	1:96:32	3–16	104	178	0	0	3.1
DMPC/DMPG	1:96:32	4–16	104	177	0	0	3.1
DMPC/DMPG	1:96:32	3–15	106	178	6	2	2.0

with the low-concentration P/L = 1:100 samples, so it was justified to assume that MAG2-F12A again had a splitting around 0 kHz (similar to the small 3 kHz splitting at P/L = 1:100). As for MAG2-F5A and MAG2-G18A, the missing splitting seems to be due to a genuine experimental problem, so we did not include them in the analysis. We nevertheless obtained a good fit from the remaining eight data points (Fig. 3, *D–F*), giving almost the same dynamics

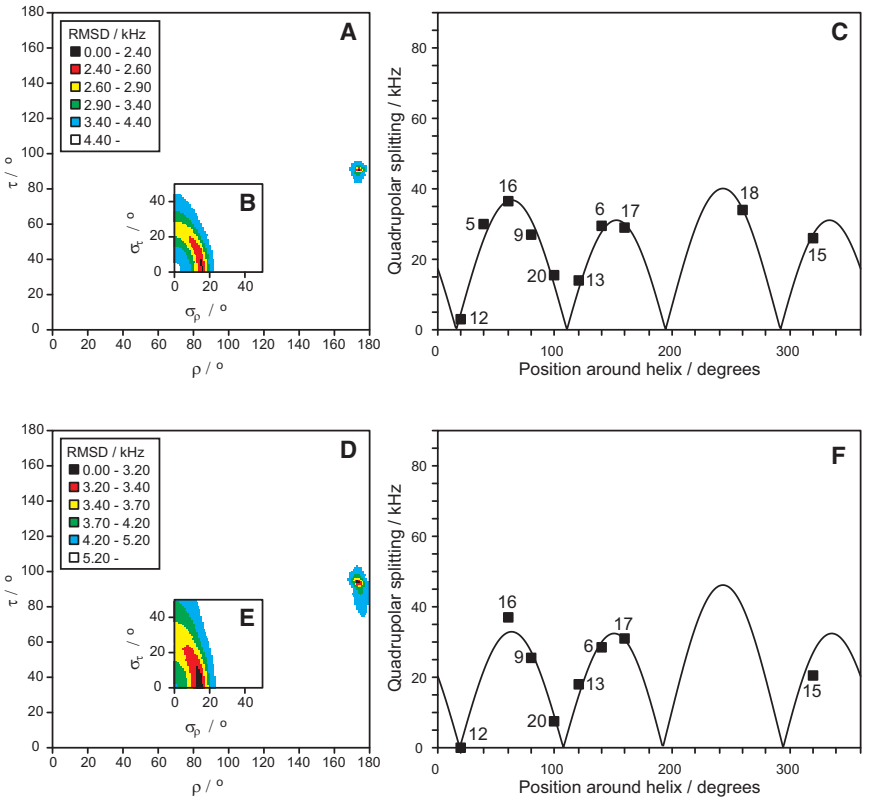

FIGURE 3 Best-fit analysis of the ^{2}H-NMR splittings from MAG2 in DMPC/DMPG (3:1). (*A–C*) Results for P/L = 1:100. (*D–F*) Results for P/L = 1:50, analogous to Fig. 2. (*A*) The RMSD plot as a function of peptide orientation shows a single well-defined minimum at $\tau = 91°$ and $\rho = 174°$. (*B*) Corresponding RMSD plot as a function of dynamical parameters (same color code as in *A*). (*C*) Helical wave plot with experimental data. (*D*) The RMSD plot shows a single well-defined minimum at $\tau = 94°$ and $\rho = 174°$. (*E*) Corresponding RMSD plot as a function of dynamical parameters (same color code as in *D*). (*F*) Helical wave plot with experimental data. To see this figure in color, go online.

and orientation as determined for P/L = 1:100 ($\tau = 94°$, $\rho = 174°$; see Table 2). (Please note that the small difference in τ of only 3° actually leads to a change in splittings of up to 8 kHz, illustrating the sensitivity of the method.) Using alternative values or completely excluding the splittings at positions 17 and 20, where the spectra are of lower quality, gave almost identical best-fit orientations (within 1–2°), as shown in Supporting Material (see Fig. S5 and Table S4). Interestingly, the flat surface orientation of MAG2 in DMPC/DMPG at both P/L = 1:100 and 1:50 is in contrast to the observed flip of the helix by 30° reported for the other two closely related peptides. Both PGLa (38–40) and MSI-103 (47,50) in DMPC/DMPG change their alignment from ~95° at low peptide concentrations to 125° at P/L = 1:50 and higher concentrations. Nonetheless, the ^{2}H-NMR result for MAG2 is perfectly in line with a previous ^{15}N-NMR study (28), which also showed an unchanged surface orientation in DMPC/DMPG (3:1) at P/L = 1:50, and only a minor difference between POPC/POPG (9:1) and DMPC/DMPG (3:1).

It was previously found that PGLa changes its orientation dramatically when it is mixed with MAG2 in a 1:1 molar ratio. This was first noted in a ^{2}H-NMR study (41) and later confirmed using ^{15}N-NMR (28,29). PGLa alone assumed a tilted state with a helix tilt angle of ~125° at P/L = 1:50, but when mixed with MAG2 in a 1:1 molar ratio, PGLa became completely inserted in DMPC/DMPG (3:1) in a transmembrane orientation with a tilt angle close to 180° (41). This was not the case, however, in POPC/POPG (28,29), and a more systematic study revealed that PGLa would only insert in the presence of MAG2 into lipid bilayers with a positive spontaneous curvature. In these systems, MAG2 also changed its orientation to a slightly more tilted state, whereas in lipids with a negative spontaneous curvature, both peptides were always found to remain flat on the surface (28). To examine the detailed response of MAG2 in the presence of PGLa, we prepared samples with MAG2 and PGLa in a 1:1 molar ratio in DMPC/DMPG (3:1) at a total P/L of 1:50, i.e., with PGLa/MAG2/DMPC/DMPG at 1:1:75:25 (see Fig. 1 *D*). As was the case for MAG2 alone in DMPC/DMPG (3:1) at P/L = 1:50, these spectra did not always give clear splittings. For MAG2-A9, MAG2-F12A, and MAG2-F16A, only a central peak was seen. We therefore left these positions out and performed a fit to the other seven data points (Fig. 4). Now, a more tilted state was found for MAG2 compared with its orientation without PGLa, namely, $\tau = 122°$, which corresponds to a change in tilt of ~30°. The azimuthal angle also changed by ~30° to $\rho = 147°$. The dynamics remained very low, similar to the behavior of MAG2 on its own, with some fluctuations in ρ but not in τ. It can be noted that according to the analysis, several of the splittings changed sign when PGLa was present, indicating quite a substantial effect on the orientation. The change in orientation into a more tilted state fits perfectly with results from a previous ^{15}N-NMR study (28), but that study was not able to detect the change in ρ.

In our previous microbiological study (45), the analogs for which the splittings could not be determined here in DMPC/DMPG at a high concentration of MAG2 (P/L = 1:50) with or without PGLa (MAG2-F5A, MAG2-F12A, and MAG2-F16A) also showed a reduced antimicrobial activity and a lower synergy with PGLa compared with MAG2-WT. However, some other analogs with lower antimicrobial activity (MAG2-L6A and MAG2-I20A) showed clear NMR splittings in the study presented here, but also retained their synergy with PGLa (45). At low peptide concentrations, where MAG2 is most likely monomeric, all analogs gave well-defined splittings and all splittings could be fitted. It is not clear why some samples did not give well-resolved splittings, but we speculate that the Phe residues may be involved in the dimerization of MAG2 with itself and/or with PGLa, and that a change from Phe to Ala could change the aggregation or mobility of MAG2 and thereby lead to a loss of ^{2}H-NMR signals.

In addition to the ^{2}H-NMR experiments, we ran all-atom MD simulations to examine the structure of MAG2, both in DMPC bilayers and in the more complex DMPC/DMPG (3:1) mixture. Several groups have previously simulated MAG2 in solution (51), with coarse-grained models (52)

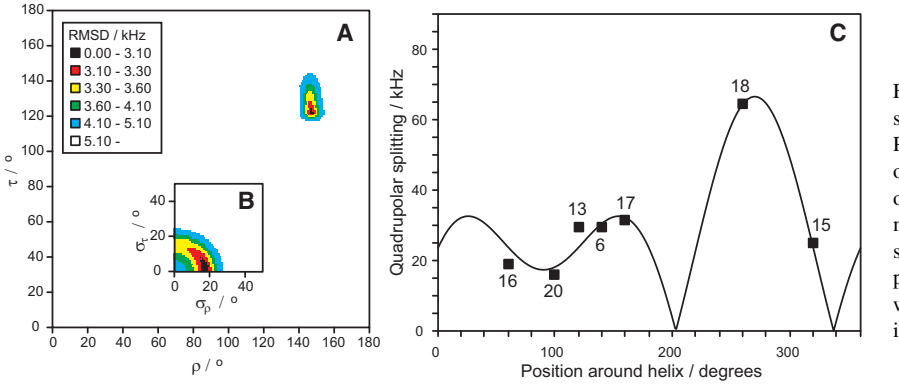

FIGURE 4 Best-fit analysis of the ^{2}H-NMR splittings from MAG2 in a 1:1 mixture with PGLa, in DMPC/DMPG (3:1) at P/L = 1:50, analogous to Fig. 2. (*A*) The RMSD plot as a function of peptide orientation shows a single well-defined minimum at $\tau = 122°$ and $\rho = 147°$. (*B*) Corresponding RMSD plot as a function of dynamical parameters (same color code as in *A*). (*C*) Helical wave plot with experimental data. To see this figure in color, go online.

or implicit membranes (53), or used MAG2 mutants or analogs (54), but very few all-atom simulations have been performed on MAG2 bound to a lipid membrane (55,56). In the two studies we are aware of that have been performed in POPC bilayers, the simulations were only 20 ns (56) and 50 ns (55) long, and the authors themselves stated that "this run time is not sufficient to equilibrate the peptide position and orientation within the bilayer" (55). Since no directly comparable simulation data were available, we thus performed a new simulation. With improved computers, much longer simulations times are now feasible, so we were able to perform one 1-μs-long simulation of MAG2 in DMPC and one 700-ns-long simulation of MAG2 in a DMPC/DMPG (3:1) mixture using recently developed force fields (57,58). Since some time is needed for any simulation to reach an equilibrium state, we performed an error analysis (as described in Supporting Materials and Methods) to determine this length of time, and then discarded the initial period up to that point. For DMPC, the first 140 ns were discarded, and for DMPC/DMPG the first 160 ns were discarded; further analyses were then done on the remaining part of the simulation.

Obviously, the results of a simulation should always be validated by comparison with experimental data, which we could obtain directly from our ^{2}H-NMR analysis. To compare the MD results with the NMR data, we back-calculated hypothetical ^{2}H-NMR quadrupole splittings from the MD trajectories and compared them with the experimental values. For each residue, the C_α-C_β bond orientation was used to determine the hypothetical splitting that would have been found by ^{2}H-NMR if this residue had been labeled as Ala-d_3. The full sets of back-calculated splittings for each position in MAG2 for each simulation are given in Table S2, and the MD splittings of the positions that were actually measured by NMR are given in Table 1 for easier comparison.

In DMPC, when we tried to fit a quadrupolar wave to the MD-derived splittings of all 23 positions, using the same method employed to fit the experimental NMR splittings described above, we found a very poor RMSD of 9.3 kHz. This was not unexpected, because the fitting method assumes an ideal α-helix, and MAG2 clearly does not form a helix along its full length in the simulation, as it unravels near the C-terminus. It can be seen in Fig. 5 that the helix is quite well defined up to residue Phe16, with the possible exception of the far N-terminus. Indeed, by narrowing down the range of positions to be used in the fit, we found that the MD-derived data from positions 3–16 gave a good fit with an RMSD of 3.7 kHz, similar to the fit to the NMR data, and further narrowing down of the range did not improve the fit. The best-fit results are summarized in Fig. 6 and Table 2. It can be noted that even when all positions were used in the fit, despite the very large RMSD, the best-fit peptide orientation was almost the same as that found when only the reduced region was fitted to obtain the better RMSD. Much to our satisfaction, the orientation obtained from the back-calculated splittings for positions 3–16 gave essentially the same peptide alignment as the fit to the experimental NMR data at P/L = 1:50, namely, the same tilt angle ($\tau \approx 94°$) and a very similar azimuthal angle ($\rho \approx 176°$). The peptide was a bit more mobile in the MD-derived fit compared with the NMR fit, with a larger σ_τ of 10–15° compared with 0–1° in the fits of NMR data.

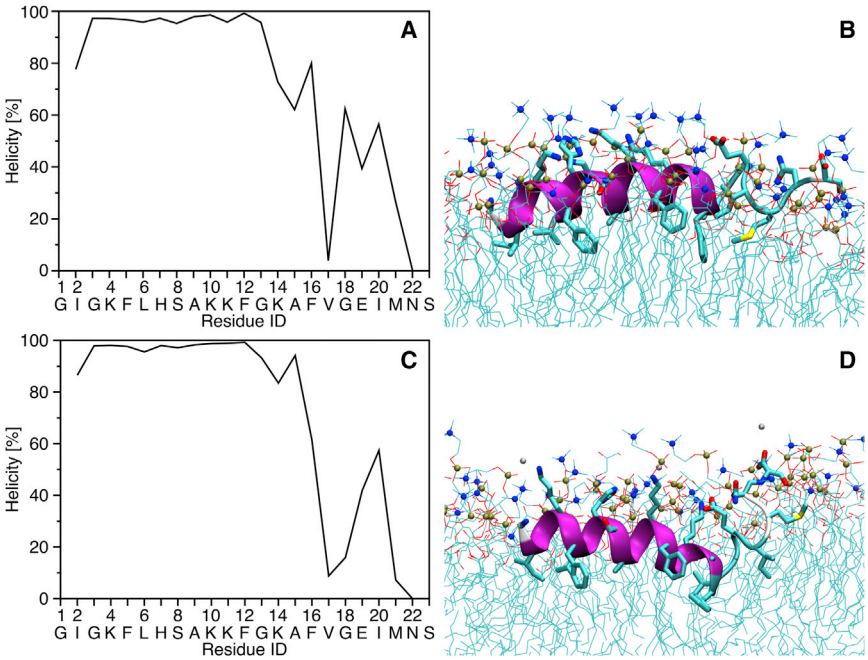

FIGURE 5 (*A*) Helicity of MAG2 from the MD simulation in DMPC, calculated from the torsion angles for each residue (helicity is undefined for the first and last residues). The percentage gives the proportion of time steps when the residue is helical, i.e., 100% means the residue is in a helical conformation during all time steps of the simulation. (*B*) Snapshot from the end of the simulation in DMPC. On the right, at the C-terminal end of the peptide, one can clearly observe unfolding starting from position 17. (*C*) Helicity of MAG2 from the MD simulation in DMPC/DMPG, calculated from the torsion angles for each residue. (*D*) Snapshot from the end of the simulation in DMPC/DMPG. To see this figure in color, go online.

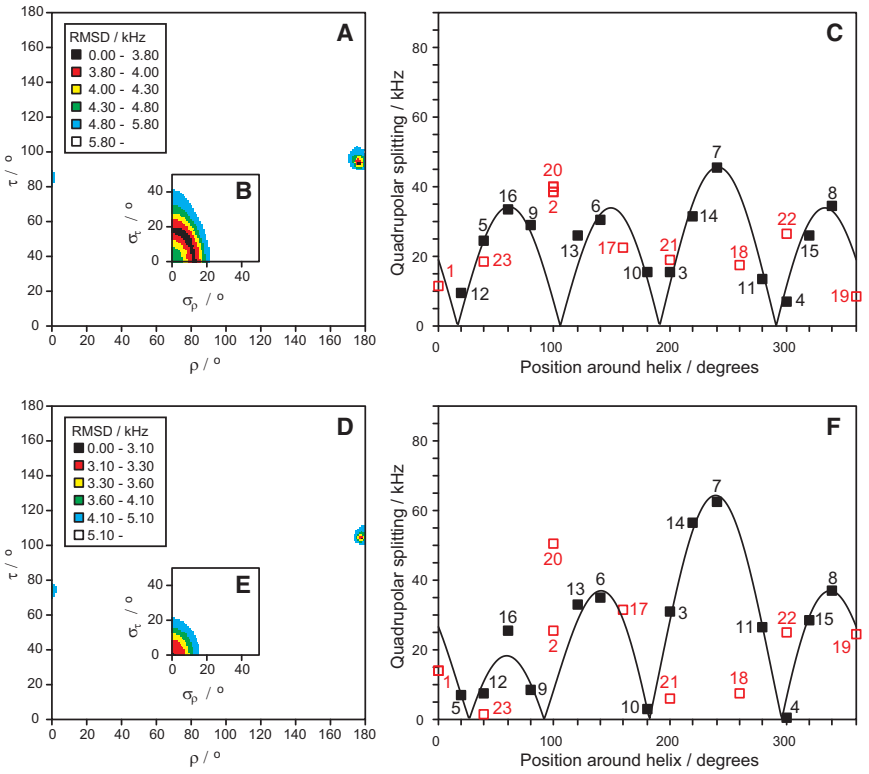

FIGURE 6 (*A–F*) Best-fit analysis of ^{2}H-NMR splittings back-calculated from the MD simulation of MAG2 in DMPC (*A–C*) and in DMPC/DMPG (3:1) (*D–F*). Only data from positions 3–16 were used, since this was the helical part of the peptide in the simulations. (*A*) The RMSD plot as a function of peptide orientation in DMPC shows a single well-defined minimum at $\tau = 94°$ and $\rho = 176°$. (*B*) Corresponding RMSD plot as a function of dynamical parameters (same color code as in *A*). (*C*) The helical wave plot shows the curve of the MD-derived splittings obtained using the best-fit parameters, together with the experimental data points. The splittings from residues that were not used in the fit are shown as open red symbols. (*D*) The RMSD plot as a function of peptide orientation in DMPC/DMPG shows a single well-defined minimum at $\tau = 104°$ and $\rho = 178°$. (*E*) RMSD plot as a function of dynamical parameters, showing less dynamics than in DMPC. (*F*) In the helical wave plot, the shape of the helical curve is different from that obtained for DMPC due to the difference in the tilt angle. To see this figure in color, go online.

When the MD simulation in DMPC/DMPG was analyzed, the back-calculated data from all 23 positions also gave a bad fit with a very high RMSD of 13.5 kHz, but narrowing down the range to positions to 3–16 gave a reasonable RMSD of 3.1 kHz. The helix tilt angle was 104°, ~10° higher than in the simulation in DMPC, whereas $\rho = 178°$ was within a few degrees of the value in DMPC. In DMPC, position 16 had been well matched to the helical curve, but in DMPC/DMPG a narrowing down of the range to 3–15 gave an even better fit with RMSD = 2.0 kHz, and almost the same orientation as obtained using 3–16.

Previous solid-state NMR analyses of various peptides from the magainin family in oriented membrane samples found no difference in helix orientation between DMPC and DMPC/DMPG mixtures. For PGLa (39) and MSI-103 (50), ^{2}H-NMR studies found no difference, and for PGLa and MAG2, ^{15}N-NMR indicated no difference between the peptide orientations in DMPC and DMPC/DMPG (28). Therefore, in this ^{2}H-NMR study of MAG2, we also expected to find no difference. However, in our two MD simulations, we found a slight difference in the tilt angle of ~10°. Notably, when compared with the NMR data obtained in DMPC/DMPG, the simulation in DMPC matched the experimental data better than the simulation in DMPC/DMPG, which used the same lipid system as the NMR samples. This seems to indicate that the simulation in DMPC is more reliable in reproducing experimental results. The splittings in the range of 3–16 were almost the same in the simulation in DMPC and in the NMR experiments, and the minor differences can be almost completely explained by the slight change in the ρ angle, which shifts the helical curve and can lead to considerable differences in splittings even for small changes in ρ, in certain regions of the curve with a steep slope (see Fig. 6). The splittings in the DMPC/DMPG simulation are quite different because the tilt angle is significantly different in this case.

The only significant difference between the simulation in DMPC and the ^{2}H-NMR data can be found for positions 17–20. Here, the back-calculated and experimental splittings differ up to 55 kHz (taking the sign into account), whereas in the range of positions 3–16 the differences are much smaller. As shown in Fig. 5, the helicity of MAG2 in the simulation is very low beyond Val-17 in DMPC, and in DMPC/DMPG even Phe-16 is not very helical, whereas the experimental splittings fit nicely to an ideal helix up to Ile-20 in DMPC/DMPG (see Fig. 3). We recently showed that the helicity found in MD simulations of peptides in membranes are highly dependent on the force field used (44). In a simulation of PGLa in a DMPC bilayer, central parts of the peptide were hardly helical at all when the OPLS force field was used, whereas the peptide was fully helical from the N- to C-terminus, with no fraying at the ends, when the CHARMM force field was used. In that study (44), the results of the CHARMM simulation were found to fit better with the solid-state NMR data, but gave unrealistically high helicity close to the ends of the peptides.

Thus, it seems that MD simulation results for peptides in membranes are still not very reliable when helicity is concerned, and that the force fields still need to be improved.

In an independent approach, we also set out to extract the τ and ρ angles directly from the simulation trajectory, as described in Supporting Materials and Methods. Here, we again used the region from positions 3–16, and found $\tau = 91^\circ$ and $\rho = 187^\circ$ in DMPC, and $\tau = 103^\circ$ and $\rho = 191^\circ$ in DMPC/DMPG. From a fit of Gaussians to the distributions of τ and ρ angles over the simulation, we obtained $\sigma_\tau = 7^\circ$ and $\sigma_\rho = 11^\circ$ in DMPC, and $\sigma_\tau = 10^\circ$ and $\sigma_\rho = 14^\circ$ in DMPC/DMPG (see Fig. 7), which are similar to the values found from the fit of back-calculated splittings from the MD, although the σ_τ value is somewhat larger than that obtained from a fit to NMR data.

Although τ in DMPC is very close to the value obtained via the MD-derived back-calculated splittings (94°), ρ is different by 11°. This deviation is due to the α parameter used to describe the helix geometry for the fit, for which we took 53.2° as the standard value (37,40,47). A detailed analysis of the α and β angles from the simulation, however, resulted in more appropriate values of $\alpha = 42^\circ$ and $\beta = 122^\circ$ (59). Using a somewhat different value for the α angle does not influence the quality of the fit, but simply shifts the resulting readout for the azimuthal rotation angle ρ. As the quadrupole splittings depend on $[\rho + \alpha]$ (see Fig. S1 and (60)), the combination of $\rho = 177^\circ$ and $\alpha = 53^\circ$ (from the fit of MD-derived splittings) is equivalent to $\rho = 187^\circ$ and $\alpha = 43^\circ$ (found directly from the MD simulation). In both cases, the orientation of the C-CD_3 bonds in the peptide in relation to the membrane normal would be exactly the same, but the position of the C_α atoms would differ. Since the quadrupole splittings measured in the experiments depend only on the orientation of the C-CD_3 bonds, the α angle should be determined separately and independently. Here, in our analysis of the NMR data, we used the value $\alpha = 53.2^\circ$, which we had also used in the past to analyze previous NMR data, as this will give us ρ angles that are compatible with earlier publications from our group. We note, however, that this choice of α is based on a static helical model (37), whereas the value from the MD simulation (59) is based on a more flexible peptide in a membrane and could therefore be more realistic. Nevertheless, the angle from the simulation obviously also depends on the force field, and by using another force field, one might find yet another value of α. The α angle from the simulation may also depend on the particular peptide and lipids used in the simulation, so it is not clear whether all previous values of ρ determined from solid-state NMR using side-chain isotope labels (^{2}H or ^{19}F) would also need to be adjusted (in studies from our group and other studies). Factually, the reliable angle determined from solid-state NMR experiments is always $[\rho + \alpha]$.

Overall, taking into account the explicable difference in α, the orientation of MAG2 obtained from the MD-derived back-calculated splittings and the orientation obtained directly from the trajectory are essentially identical. Fig. 7 *A* shows the time evolution of τ and ρ in DMPC. The first 140 ns were discarded in the statistical evaluation, as discussed above. We therefore give all splittings and angles as averages over the last 860 ns of the simulation. Fig. 7 *B* shows the resulting distributions of τ and ρ in

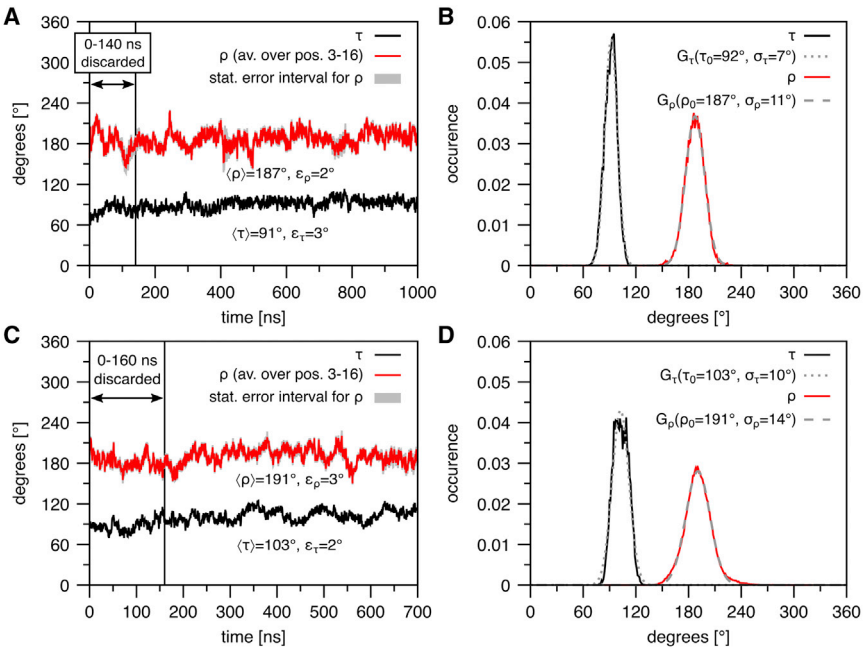

FIGURE 7 (*A–D*) Independent evaluation of τ and ρ from the MD trajectories of (*A* and *B*) MAG2 in DMPC and (*C* and *D*) MAG2 in DMPC/DMPG. (*A*) τ (lower curve) and ρ (upper curve) were calculated as averages from $t =$ 140 ns until the end of the simulation at 1 μs; their values are $\langle\tau\rangle = 91^\circ \pm 3^\circ$ and $\langle\rho\rangle = 187^\circ \pm 2^\circ$. ρ at each time t was calculated as the average (in *red*) over the values obtained from positions 3–16, projected to position 12. The gray area denotes the statistical error on the value for each time step. The first 140 ns were discarded as the equilibration phase (a detailed explanation is given in Supporting Materials and Methods). (*B*) Histograms of τ and ρ obtained from the last 860 ns of the simulation and their fits to Gaussian distributions, $G_\alpha(\alpha_0, \sigma_\alpha, x) \propto \exp[-(x - \alpha_0)^2/(2\sigma_\alpha)]$, $\alpha \in [\tau, \rho]$. Distributions are normalized to an integral of one. As expected from NMR, ρ has a wider distribution than τ. (*C*) τ and ρ were calculated as averages from $t = 160$ ns until the end of the simulation at 700 ns; their values are $\langle\tau\rangle = 103^\circ \pm 2^\circ$ and $\langle\rho\rangle = 191^\circ \pm 3^\circ$. The first 160 ns were discarded as the equilibration time. (*D*) Histograms of τ and ρ obtained from the last 540 ns of the simulation and their fits to Gaussian distributions. To see this figure in color, go online.

DMPC. The distribution for τ is much narrower than that for ρ, which nicely confirms the experimental findings by ^{2}H-NMR. Fig. 7, *C* and *D*, show the time evolution and histograms of τ and ρ in DMPC/DMPG (3:1), respectively, where the first 160 ns have been discarded.

We found a difference of ~10° in the tilt angle of MAG2 when we compared the simulations in DMPC and DMPC/DMPG. Given the overriding significance of the experimental ^{2}H-NMR data, we attribute this slight difference in the MD simulations to a suboptimal force field that was available for the DMPC/DMPG mixture. Generally, it can be said that electrostatic interactions are hard to simulate, and this can lead to problems with the charged DMPG lipids. In addition, the data used to calibrate MD simulation parameters (e.g., area per lipid) are scarcely available for lipid mixtures, meaning that simulations are more reliable and robust when a single lipid is used. Nevertheless, we wanted to know whether there are any genuine reasons that could explain the slight increase of τ in DMPC/DMPG, which implies that the C-terminal part of the peptide has dipped more into the membrane. Therefore, we analyzed the MD trajectories to find out whether the difference might be due to an electrostatic attraction between the negatively charged residues in the unfolded C-terminus of MAG2 (Glu-19 and the free C-terminal Ser-23) and the positively charged choline groups of DMPC. In DMPC/DMPG (3:1), there were 25% fewer positive charges in the headgroups compared with pure DMPC, which could lead to a weaker attraction of the C-terminus (but stronger overall binding of the remaining cationic peptide). When we counted the contacts (distances below 5 Å; numbers have been normalized to the simulation time) between the oxygens of Glu-19 and the nitrogen atoms of DMPC, we found 2.8 times more contacts in pure DMPC than in DMPC/DMPG (3:1), even though there were only 1.3 times more DMPC lipids. For the contacts between Ser-23 and the choline groups of DMPC, the effect was less pronounced: there were only 1.7 times more contacts in pure DMPC than in the DMPC/DMPG mixture. In DMPC/DMPG, the average position of the oxygens of Glu-19 was 3.2 Å below the average position of the phosphorus, whereas in DMPC the same oxygens were approximately at the same height as the average phosphorus position, and the errors indicate a much higher variability (for details of the error calculation method used, see Supporting Material). The tendency to tilt probably stems from Phe-16, which tries to bury its aromatic side chain in the hydrophobic core of the membrane. The tension that is created by these opposite driving forces might also be responsible for the rupture of the helical structure at position 17 in the simulations. According to the NMR experiment, however, the peptide has a much longer continuous helical segment up to residue 20. This means that the vulnerability of the helical structure to this tension must be caused by the force field used in the MD simulation. This could be explained by a general imperfect representation of helicity as discussed above, a suboptimal description of electrostatic interactions resulting in too-strong attractive forces, or a combination of both.

In the MD simulations, only a single peptide was present, so the simulations represent the situation of a monomeric MAG2 molecule far from any other peptides in the membrane. In a real membrane under antimicrobial attack, many peptides are present that may interact with each other. The simulation results fit very well with the experiments done in POPC/POPG at P/L = 1:50, and also with experiments done in DMPC/DMPG at 1:100 and 1:50. It thus seems that magainin-magainin interactions are not important under these conditions. However, in the presence of PGLa (given the same total peptide concentration), the orientation of MAG2 changes considerably, indicating a strong interaction between these two synergistic partners. This observation not only confirms previous reports of synergy between these two peptides (18,20,21,23,61) but also suggests the possible formation of heterodimers (21,23). Since the orientation of PGLa in the presence of MAG2 changes even more dramatically into a transmembrane orientation, we propose that a complex is formed in which MAG2 is partially inserted into the membrane and PGLa is fully inserted.

In MAG2, both terminal residues are free and charged, and on its own the peptide lies flat on the membrane surface with a helix tilt angle very close to 90°. In PGLa, on the other hand, the C-terminus is amidated, and at high concentrations ($\geq$1:50) in saturated lipids (e.g., DMPC or DLPC) a tilt angle of ~125° has been found, with the uncharged C-terminus being more deeply inserted into the membrane than the charged N-terminus (38–40). The same tilting behavior was also reported for MSI-103, another AMP that has a sequence similar to that of PGLa and also carries an amidated C-terminus (47,50). When in contact with PGLa, MAG2 also flips into a tilted state such that its C-terminus lies deeper in the membrane than its N-terminus. Notably, the C-terminus of MAG2 carries two negative charges: Glu-19 and the free C-terminus. It is thus tempting to speculate that the anionic C-terminal region of MAG2 engages in close molecular contact with positive groups on PGLa (see Fig. S6). In one study, a reduced synergy was observed for the mutant MAG2-E19Q-amide, in which both negative charges of MAG2 are removed (21). According to a cross-linking study, it is most likely that PGLa and MAG2 form a heterodimer with the C-termini in contact with each other (23), which would fit well with our results. It thus seems plausible that salt bridges could be formed, which would neutralize the negative charges on MAG2 and allow its C-terminal region to participate in a stable pore. If at the same time some of the five positive charges on PGLa are neutralized by MAG2, this should make it easier for the PGLa helices to assemble into the actual pore, which is presumably of the toroidal wormhole type. We present in Fig. 8 a plausible model of such a pore, in

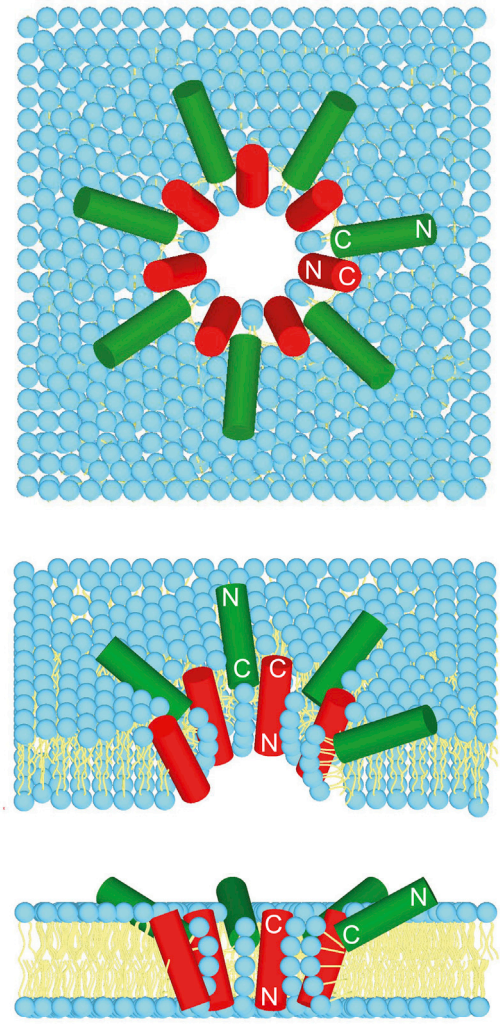

FIGURE 8 Hypothetical model of a toroidal pore made up of PGLa (*red transmembrane cylinders*) and MAG2 (*green cylinders on the surface*) in a lipid membrane. The actual tilt angles of the peptides were determined by ^{2}H-NMR in 1:1 peptide mixtures (this work and (20,41)). A likely contact between the C-termini of the two peptides in each heterodimer was suggested in a previous study (23). To see this figure in color, go online.

which the peptide tilt angles are compatible with solid-state NMR, and in which the heterodimers have been constructed with a contact between the C-termini of the two peptides.

At present, we are not yet able to perform simulations of PGLa and MAG2 together in a membrane. Several molecules of each kind presumably are needed to form a pore, and simulations with all-atom models are still too slow to allow simulations on sufficiently long timescales to study pore formation. In a recent study (62), a coarse-grained MD simulation using 12 copies of each peptide revealed electrostatic interactions between the negative charges of MAG2 and the positive charges close to the C-terminus of PGLa. In that study, a reorientation of PGLa was observed in the presence of MAG2, and when the negative charges of MAG2 were removed in the simulation, no reorientation of PGLa was observed. Hence, the simulation indicated that the reorientation of PGLa depends on electrostatic interactions with MAG2 (62). The coarse-grained simulation did not fit perfectly with NMR experiments, as PGLa was not seen to flip into an inserted state, which was shown by ^{2}H- and ^{15}N-NMR results known at the time. Instead, PGLa only changed its angle to a tilted state ($\tau \approx 120°$), and the MAG2 orientation also changed slightly (from $\tau \approx 90°$ to $\tau \approx 100°$). In a more recent all-atom simulation, very long simulations of PGLa and MAG2 in lipid bilayers, covering 5–9 μs, were performed on the Anton supercomputer (63). This time frame was not sufficient to let pores form spontaneously, so tetrameric bundles of PGLa, MAG2, or heterotetramers were initially inserted in a transmembrane orientation into DMPC or DMPC/DMPG (3:1) lipid bilayers. It was found that both parallel and antiparallel heterodimers starting in a pore configuration were stable over the simulation time (63). As in the coarse-grained simulation, favorable interactions were found between E19 of MAG2 and the C-terminal Lys of PGLa (63). However, both MAG2 and PGLa had a transmembrane orientation in the simulation, whereas NMR results show that only PGLa is inserted into the membrane in the PGLa/MAG2 mixture, with MAG2 being only slightly tilted (28,29). It seems likely that all-atom simulations are better suited than coarse-grained simulations to elucidate the peptide-peptide and peptide-lipid interactions involved in the pore formation and synergy of PGLa/MAG2, but so far the starting structure of the pore must be built "by hand" and is not well understood. Based on the new, to our knowledge, experimental and orientational data presented here, future all-atom simulations using improved simulation hardware should be able to lead to a better understanding of the PGLa-MAG2 complex that is responsible for the synergy between the two peptides.

SUPPORTING MATERIAL

Supporting Materials and Methods, seven figures, and four tables are available at http://www.biophysj.org/biophysj/supplemental/S0006-3495(16)30939-0.

AUTHOR CONTRIBUTIONS

E.S. and A.S.U. designed research. E.S., D.H., J.Z., and P.W. performed experiments. S.R. performed simulations. E.S. and S.R. analyzed data. E.S., S.R., and A.S.U. wrote the manuscript. All of the authors discussed the data and reviewed the manuscript.

ACKNOWLEDGMENTS

We thank Simon Hartweck and Daniel Gauder for help in preparing Fig. 8. We thank Dr. Stephan Grage for fruitful discussions, Andrea Eisele and Kerstin Scheubeck for technical support with the peptide synthesis, and Markus Schmitt for help with the NMR infrastructure.

This study was supported by a grant from the DFG-Center for Functional Nanostructures (TP E1.2).

SUPPORTING REFERENCES

References (64–76) appear in the Supporting Material.

REFERENCES

1. Boman, H. G. 1991. Antibacterial peptides: key components needed in immunity. *Cell.* 65:205–207.
2. Zasloff, M. 2002. Antimicrobial peptides of multicellular organisms. *Nature.* 415:389–395.
3. Peschel, A., and H. G. Sahl. 2006. The co-evolution of host cationic antimicrobial peptides and microbial resistance. *Nat. Rev. Microbiol.* 4:529–536.
4. Oren, Z., and Y. Shai. 1998. Mode of action of linear amphipathic α-helical antimicrobial peptides. *Biopolymers.* 47:451–463.
5. Huang, H. W. 2000. Action of antimicrobial peptides: two-state model. *Biochemistry.* 39:8347–8352.
6. Matsuzaki, K. 1998. Magainins as paradigm for the mode of action of pore forming polypeptides. *Biochim. Biophys. Acta.* 1376:391–400.
7. Sühnel, J. 1990. Evaluation of synergism or antagonism for the combined action of antiviral agents. *Antiviral Res.* 13:23–39.
8. Yan, H., and R. E. W. Hancock. 2001. Synergistic interactions between mammalian antimicrobial defense peptides. *Antimicrob. Agents Chemother.* 45:1558–1560.
9. Zasloff, M. 1987. Magainins, a class of antimicrobial peptides from *Xenopus* skin: isolation, characterization of two active forms, and partial cDNA sequence of a precursor. *Proc. Natl. Acad. Sci. USA.* 84:5449–5453.
10. Murzyn, K., and M. Pasenkiewicz-Gierula. 2003. Construction of a toroidal model for the magainin pore. *J. Mol. Model.* 9:217–224.
11. Yang, L., T. M. Weiss, …, H. W. Huang. 2000. Crystallization of antimicrobial pores in membranes: magainin and protegrin. *Biophys. J.* 79:2002–2009.
12. Matsuzaki, K., K. Sugishita, …, K. Miyajima. 1997. Interactions of an antimicrobial peptide, magainin 2, with outer and inner membranes of Gram-negative bacteria. *Biochim. Biophys. Acta.* 1327:119–130.
13. Ludtke, S. J., K. He, …, H. W. Huang. 1996. Membrane pores induced by magainin. *Biochemistry.* 35:13723–13728.
14. Maloy, W. L., and U. P. Kari. 1995. Structure-activity studies on magainins and other host defense peptides. *Biopolymers.* 37:105–122.
15. Ludtke, S., K. He, and H. Huang. 1995. Membrane thinning caused by magainin 2. *Biochemistry.* 34:16764–16769.
16. Hunt, L. T., and W. C. Barker. 1988. Relationship of promagainin to three other prohormones from the skin of *Xenopus laevis*: a different perspective. *FEBS Lett.* 233:282–288.
17. Terry, A. S., L. Poulter, …, B. W. Gibson. 1988. The cDNA sequence coding for prepro-PGS (prepro-magainins) and aspects of the processing of this prepro-polypeptide. *J. Biol. Chem.* 263:5745–5751.
18. Westerhoff, H. V., M. Zasloff, …, D. Juretić. 1995. Functional synergism of the magainins PGLa and magainin-2 in *Escherichia coli,* tumor cells and liposomes. *Eur. J. Biochem.* 228:257–264.
19. Haney, E. F., H. N. Hunter, …, H. J. Vogel. 2009. Solution NMR studies of amphibian antimicrobial peptides: linking structure to function? *Biochim. Biophys. Acta.* 1788:1639–1655.
20. Strandberg, E., P. Tremouilhac, …, A. S. Ulrich. 2009. Synergistic transmembrane insertion of the heterodimeric PGLa/magainin 2 complex studied by solid-state NMR. *Biochim. Biophys. Acta.* 1788:1667–1679.
21. Matsuzaki, K., Y. Mitani, …, K. Miyajima. 1998. Mechanism of synergism between antimicrobial peptides magainin 2 and PGLa. *Biochemistry.* 37:15144–15153.
22. Juretic, D. 1990. Antimicrobial peptides of the magainin family: membrane depolarization studies on *E. coli* and cytochrome oxidase liposomes. *Stud. Biophy.* 138:79–86.
23. Hara, T., Y. Mitani, …, K. Matsuzaki. 2001. Heterodimer formation between the antimicrobial peptides magainin 2 and PGLa in lipid bilayers: a cross-linking study. *Biochemistry.* 40:12395–12399.
24. Strandberg, E., and A. S. Ulrich. 2004. NMR methods for studying membrane-active antimicrobial peptides. *Concepts Magn. Reson. A.* 23A:89–120.
25. Ulrich, A. S., P. Wadhwani, …, S. L. Grage. 2006. Solid-state ^{19}F-nuclear magnetic resonance analysis of membrane-active peptides. *In* NMR Spectroscopy of Biological Solids. A. Ramamoorthy, editor. CRC Press, Boca Raton, FL, pp. 215–236.
26. Bechinger, B. 2011. Insights into the mechanisms of action of host defence peptides from biophysical and structural investigations. *J. Pept. Sci.* 17:306–314.
27. Wadhwani, P., and E. Strandberg. 2009. Structure analysis of membrane-active peptides using ^{19}F-labeled amino acids and solid-state NMR. *In* Fluorine in Medicinal Chemistry and Chemical Biology. I. Ojima, editor. Blackwell Publishing, London, pp. 463–493.
28. Strandberg, E., J. Zerweck, …, A. S. Ulrich. 2013. Synergistic insertion of antimicrobial magainin-family peptides in membranes depends on the lipid spontaneous curvature. *Biophys. J.* 104:L9–L11.
29. Salnikov, E. S., and B. Bechinger. 2011. Lipid-controlled peptide topology and interactions in bilayers: structural insights into the synergistic enhancement of the antimicrobial activities of PGLa and magainin 2. *Biophys. J.* 100:1473–1480.
30. Bechinger, B., M. Zasloff, and S. J. Opella. 1998. Structure and dynamics of the antibiotic peptide PGLa in membranes by solution and solid-state nuclear magnetic resonance spectroscopy. *Biophys. J.* 74:981–987.
31. Bechinger, B., Y. Kim, …, S. J. Opella. 1991. Orientations of amphipathic helical peptides in membrane bilayers determined by solid-state NMR spectroscopy. *J. Biomol. NMR.* 1:167–173.
32. Bechinger, B., M. Zasloff, and S. J. Opella. 1993. Structure and orientation of the antibiotic peptide magainin in membranes by solid-state nuclear magnetic resonance spectroscopy. *Protein Sci.* 2:2077–2084.
33. Ramamoorthy, A., F. M. Marassi, …, S. J. Opella. 1995. Three-dimensional solid-state NMR spectroscopy of a peptide oriented in membrane bilayers. *J. Biomol. NMR.* 6:329–334.
34. Lee, D. K., J. S. Santos, and A. Ramamoorthy. 1999. Application of one-dimensional dipolar shift solid-state NMR spectroscopy to study the backbone conformation of membrane-associated peptides in phospholipid bilayers. *J. Phys. Chem. B.* 103:8383–8390.
35. Marassi, F. M., C. Ma, …, S. J. Opella. 1999. The roles of homonuclear line narrowing and the ^{1}H amide chemical shift tensor in structure determination of proteins by solid-state NMR spectroscopy. *Appl. Magn. Reson.* 17:433–447.
36. Marassi, F. M., C. Ma, …, S. J. Opella. 2000. Three-dimensional solid-state NMR spectroscopy is essential for resolution of resonances from in-plane residues in uniformly ^{15}N-labeled helical membrane proteins in oriented lipid bilayers. *J. Magn. Reson.* 144:156–161.
37. Glaser, R. W., C. Sachse, …, A. S. Ulrich. 2004. Orientation of the antimicrobial peptide PGLa in lipid membranes determined from ^{19}F-NMR dipolar couplings of 4-CF_3-phenylglycine labels. *J. Magn. Reson.* 168:153–163.
38. Glaser, R. W., C. Sachse, …, A. S. Ulrich. 2005. Concentration-dependent realignment of the antimicrobial peptide PGLa in lipid membranes observed by solid-state ^{19}F-NMR. *Biophys. J.* 88:3392–3397.
39. Tremouilhac, P., E. Strandberg, …, A. S. Ulrich. 2006. Conditions affecting the re-alignment of the antimicrobial peptide PGLa in membranes as monitored by solid state ^{2}H-NMR. *Biochim. Biophys. Acta.* 1758:1330–1342.
40. Strandberg, E., P. Wadhwani, …, A. S. Ulrich. 2006. Solid-state NMR analysis of the PGLa peptide orientation in DMPC bilayers: structural fidelity of ^{2}H-labels versus high sensitivity of ^{19}F-NMR. *Biophys. J.* 90:1676–1686.
41. Tremouilhac, P., E. Strandberg, …, A. S. Ulrich. 2006. Synergistic transmembrane alignment of the antimicrobial heterodimer PGLa/magainin. *J. Biol. Chem.* 281:32089–32094.

42. Afonin, S., S. L. Grage, …, A. S. Ulrich. 2008. Temperature-dependent transmembrane insertion of the amphiphilic peptide PGLa in lipid bilayers observed by solid state ^{19}F NMR spectroscopy. *J. Am. Chem. Soc.* 130:16512–16514.

43. Reißer, S., E. Strandberg, …, A. S. Ulrich. 2014. 3D hydrophobic moment vectors as a tool to characterize the surface polarity of amphiphilic peptides. *Biophys. J.* 106:2385–2394.

44. Ulmschneider, J. P., J. C. Smith, …, E. Strandberg. 2012. Reorientation and dimerization of the membrane-bound antimicrobial peptide PGLa from microsecond all-atom MD simulations. *Biophys. J.* 103:472–482.

45. Strandberg, E., J. Zerweck, …, A. S. Ulrich. 2015. Influence of hydrophobic residues on the activity of the antimicrobial peptide magainin 2 and its synergy with PGLa. *J. Pept. Sci.* 21:436–445.

46. Bechinger, B., M. Zasloff, and S. J. Opella. 1992. Structure and interactions of magainin antibiotic peptides in lipid bilayers: a solid-state nuclear magnetic resonance investigation. *Biophys. J.* 62:12–14.

47. Strandberg, E., D. Tiltak, …, A. S. Ulrich. 2012. Lipid shape is a key factor for membrane interactions of amphipathic helical peptides. *Biochim. Biophys. Acta.* 1818:1764–1776.

48. Strandberg, E., and A. S. Ulrich. 2015. AMPs and OMPs: is the folding and bilayer insertion of β-stranded outer membrane proteins governed by the same biophysical principles as for α-helical antimicrobial peptides? *Biochim. Biophys. Acta.* 1848:1944–1954.

49. Afonin, S., R. W. Glaser, …, A. S. Ulrich. 2014. ^{19}F NMR screening of unrelated antimicrobial peptides shows that membrane interactions are largely governed by lipids. *Biochim. Biophys. Acta.* 1838:2260–2268.

50. Strandberg, E., N. Kanithasen, …, A. S. Ulrich. 2008. Solid-state NMR analysis comparing the designer-made antibiotic MSI-103 with its parent peptide PGLa in lipid bilayers. *Biochemistry.* 47:2601–2616.

51. Mehrnejad, F., H. Naderi-Manesh, and B. Ranjbar. 2007. The structural properties of magainin in water, TFE/water, and aqueous urea solutions: molecular dynamics simulations. *Proteins.* 67:931–940.

52. Woo, H. J., and A. Wallqvist. 2011. Spontaneous buckling of lipid bilayer and vesicle budding induced by antimicrobial peptide magainin 2: a coarse-grained simulation study. *J. Phys. Chem. B.* 115:8122–8129.

53. Zhan, H., and T. Lazaridis. 2012. Influence of the membrane dipole potential on peptide binding to lipid bilayers. *Biophys. Chem.* 161:1–7.

54. Leontiadou, H., A. E. Mark, and S. J. Marrink. 2006. Antimicrobial peptides in action. *J. Am. Chem. Soc.* 128:12156–12161.

55. Kandasamy, S. K., and R. G. Larson. 2006. Effect of salt on the interactions of antimicrobial peptides with zwitterionic lipid bilayers. *Biochim. Biophys. Acta.* 1758:1274–1284.

56. Kandasamy, S. K., and R. G. Larson. 2004. Binding and insertion of alpha-helical anti-microbial peptides in POPC bilayers studied by molecular dynamics simulations. *Chem. Phys. Lipids.* 132:113–132.

57. Jämbeck, J. P., and A. P. Lyubartsev. 2012. Derivation and systematic validation of a refined all-atom force field for phosphatidylcholine lipids. *J. Phys. Chem. B.* 116:3164–3179.

58. Lindorff-Larsen, K., S. Piana, …, D. E. Shaw. 2010. Improved side-chain torsion potentials for the Amber ff99SB protein force field. *Proteins.* 78:1950–1958.

59. Reißer, S. 2014. Computational studies of membrane-active antimicrobial peptides and comparison with NMR data. PhD thesis, Fakultät für Chemie und Biowissenschaften, Karlsruhe Institute of Technology, Karlsruhe, Germany.

60. Strandberg, E., S. Özdirekcan, …, J. A. Killian. 2004. Tilt angles of transmembrane model peptides in oriented and non-oriented lipid bilayers as determined by ^{2}H solid-state NMR. *Biophys. J.* 86:3709–3721.

61. Vaz Gomes, A., A. de Waal, …, H. V. Westerhoff. 1993. Electric potentiation, cooperativity, and synergism of magainin peptides in protein-free liposomes. *Biochemistry.* 32:5365–5372.

62. Han, E., and H. Lee. 2015. Synergistic effects of magainin 2 and PGLa on their heterodimer formation, aggregation, and insertion into the bilayer. *RSC Advances.* 5:2047–2055.

63. Pino-Angeles, A., J. M. Leveritt, 3rd, and T. Lazaridis. 2016. Pore structure and synergy in antimicrobial peptides of the magainin family. *PLOS Comput. Biol.* 12:e1004570.

64. Fields, G. B., and R. L. Noble. 1990. Solid phase peptide synthesis utilizing 9-fluorenylmethoxycarbonyl amino acids. *Int. J. Pept. Protein Res.* 35:161–214.

65. Rance, M., and R. A. Byrd. 1983. Obtaining high-fidelity spin-1/2 powder spectra in anisotropic media - phase-cycled Hahn echo spectroscopy. *J. Magn. Reson.* 52:221–240.

66. Davis, J. H., K. R. Jeffrey, …, T. P. Higgs. 1976. Quadrupolar echo deuteron magnetic resonance spectroscopy in ordered hydrocarbon chains. *Chem. Phys. Lett.* 42:390–394.

67. Davis, J. H. 1983. The description of membrane lipid conformation, order and dynamics by ^{2}H-NMR. *Biochim. Biophys. Acta.* 737:117–171.

68. Strandberg, E., S. Esteban-Martín, …, A. S. Ulrich. 2009. Orientation and dynamics of peptides in membranes calculated from ^{2}H-NMR data. *Biophys. J.* 96:3223–3232.

69. Strandberg, E., and A. S. Ulrich. 2014. Dynamic structure analysis of peptides in membranes by solid-state NMR. *In* Advances in Biological Solid-State NMR: Proteins and Membrane-Active Peptides. F. Separovic and A. Naito, editors. Royal Society of Chemistry, London, pp. 304–319.

70. Jorgensen, W. L., J. Chandrasekhar, …, M. L. Klein. 1983. Comparison of simple potential functions for simulating liquid water. *J. Chem. Phys.* 79:926–935.

71. Case, D. A., T. A. Darden, …, P. A. Kollman. 2012. AMBER 12. University of California, San Francisco.

72. Nosé, S. 1984. A molecular dynamics method for simulations in the canonical ensemble. *Mol. Phys.* 52:255–268.

73. Parrinello, M., and A. Rahman. 1981. Polymorphic transitions in single crystals—a new molecular dynamics method. *J. Appl. Phys.* 52:7182–7190.

74. Hess, B., H. Bekker, …, J. G. E. M. Fraaije. 1997. LINCS: a linear constraint solver for molecular simulations. *J. Comput. Chem.* 18: 1463–1472.

75. Darden, T., D. York, and L. Pedersen. 1993. Particle mesh Ewald—an $N\bullet\log(N)$ method for Ewald sums in large systems. *J. Chem. Phys.* 98:10089–10092.

76. Hess, B. 2002. Determining the shear viscosity of model liquids from molecular dynamics simulations. *J. Chem. Phys.* 116:209–217.

Biophysical Journal, Volume *111*

Supplemental Information

^{2}H-NMR and MD Simulations Reveal Membrane-Bound Conformation of Magainin 2 and Its Synergy with PGLa

Erik Strandberg, Diana Horn, Sabine Reißer, Jonathan Zerweck, Parvesh Wadhwani, and Anne S. Ulrich

Biophysical Journal, Volume *111*
Supporting Material

^{2}H-NMR and MD Simulations Reveal Membrane-Bound Conformation of Magainin 2 and Its Synergy with PGLa

Erik Strandberg,[1] Diana Horn,[2] Sabine Reißer,[1,3] Jonathan Zerweck,[2] Parvesh Wadhwani,[1] Anne S. Ulrich[1,2,*]

[1] Institute of Biological Interfaces (IBG-2), [2] Institute of Organic Chemistry, and [3] Institute of Physical Chemistry, Karlsruhe Institute of Technology, Karlsruhe, Germany;

* Corresponding author. Email: anne.ulrich@kit.edu

MATERIALS AND METHODS

Materials

All Fmoc protected amino acids where purchased from Iris Biotech GmbH (Marktredwitz, Germany) or Novabiochem (Merck Chemicals Ltd, Nottingham, UK), except for 3,3,3-$^2H_3$-*L*-alanine (Ala-d_3), which was purchased from Cambridge Isotope Laboratories (Andover, USA). Deuterium-depleted water was from Acros Organics (Geel, Belgium), and other solvents were from Acros Organics, Merck (Darmstadt, Germany), Fisher Scientific (Schwerte, Germany), or Biosolve (Valkenswaard, The Netherlands). The lipids 1,2-dimyristoyl-*sn*-glycero-3-phosphatidylcholine (DMPC), 1,2-dimyristoyl-*sn*-glycero-3-phosphatidylglycerol (DMPG), 1-palmitoyl-2-oleoyl-*sn*-glycero-3-phosphatidylcholine (POPC), and 1-palmitoyl-2-oleoyl-*sn*-glycero-3-phosphatidylglycerol (POPG) were purchased from Avanti Polar Lipids (Alabaster, AL, USA).

Peptide synthesis

Ala-d_3 was incorporated at specific positions in magainin 2 (MAG2) with the amino acid sequence GIGKFLHSAKKFGKAFVGEIMNS (**Table S1**). For peptide synthesis, standard Fmoc solid phase protocols were used (1), as previously described in detail (2).

Table S1. Synthesized peptides used in this study.

Peptide	**Substituted position**	**Sequence**
MAG2-WT	-	GIGKFLHSAKKFGKAFVGEIMNS
MAG2-F5A	Phe-5	GIGK-**Ala-d_3**-LHSAKKFGKAFVGEIMNS
MAG2-L6A	Leu-6	GIGKF-**Ala-d_3**-HSAKKFGKAFVGEIMNS
MAG2-A9	Ala-9	GIGKFLHS-**Ala-d_3**-KKFGKAFVGEIMNS
MAG2-F12A	Phe-12	GIGKFLHSAKK-**Ala-d_3**-GKAFVGEIMNS
MAG2-G13A	Gly-13	GIGKFLHSAKKF-**Ala-d_3**-KAFVGEIMNS
MAG2-A15	Ala-15	GIGKFLHSAKKFGK-**Ala-d_3**-FVGEIMNS
MAG2-F16A	Phe-16	GIGKFLHSAKKFGKA-**Ala-d_3**-VGEIMNS
MAG2-V17A	Val-17	GIGKFLHSAKKFGKAF-**Ala-d_3**-GEIMNS
MAG2-G18A	Gly-18	GIGKFLHSAKKFGKAFV-**Ala-d_3**-EIMNS
MAG2-I20A	Ile-20	GIGKFLHSAKKFGKAFVGE-**Ala-d_3**-MNS
PGLa	-	GMASKAGAIAGKIAKVALKAL-NH_2

Solid-state NMR

NMR sample preparation. Usually 0.5-1 mg of ^{2}H-labeled peptide was used in each sample, together with appropriate amounts of lipids to obtain the desired P/L ratio. In samples including PGLa, around 0.5 mg of the ^{2}H-labeled MAG2 analog and an equimolar amount of unlabeled PGLa was used. In short, oriented NMR samples were prepared by co-dissolving the lipid and peptide, spreading the mixture on 9 mm × 7.5 mm × 0.08 mm glass plates (Marienfeld, Lauda-Königshofen, Germany), drying to remove the solvent, and subsequent hydration at 48°C in 96% relative humidity using a saturated solution of K_2SO_4 in deuterium-depleted water (DDW) for 16-20 h. Due to problems with peptide aggregation and getting well-resolved NMR splittings at high P/L, several different methods were tried. In the *standard method* (method 1), which worked well in POPC/POPC and at P/L=1:100, the lipids were dissolved separately in 200 µl

$CHCl_3$/MeOH (1/1 v/v) and mixed in one vessel with vortexing and sonication. Peptides were dissolved in 100 µl MeOH and then mixed into the lipid solution. In some cases, when the solution was not clear, 20 µl DDW was added, and the solution was vortexed and sonicated. This solution was then spread on glass plates. In the *MLV method* (method 2), a peptide-lipid solution was prepared as in the standard method. This solution was dried under argon gas to a film and then dried further in vacuum for 1 h. The dry film was hydrated with 105 µl DDW, mixed, centrifuged, and freeze-thawed five times, to get a homogeneous, milk-like suspension. This suspension was spread onto the glass plates, which were dried in air >1 h and then under vacuum for 22 h to remove all water completely before hydration. In the *two-step method* (method 3), the peptides were first dissolved in MeOH, and after vortexing and sonification the peptide solution was spread on glass plates and air-dried. Then the lipids were dissolved in $CHCl_3$/MeOH, and after vortexing and sonication the lipid solution was spread on the glass plates on top of the peptide film. After air-drying the plates were dried under vacuum for 22 h before hydration.

Experimental parameters. Solid-state NMR experiments were carried out on 500 MHz and 600 MHz Bruker Avance NMR spectrometers (Bruker Biospin, Karlsruhe, Germany). ^{31}P-NMR was performed using a Hahn-echo sequence with ^{1}H decoupling (3), and ^{2}H-NMR was performed with a solid-echo sequence (4). Typical 90º pulse lengths were 4-5 µs. Further NMR experimental details have been published previously (5). The oriented samples were measured with the bilayer normal parallel to the external magnetic field.

NMR data analysis. The orientation of a helical peptide in the membrane can be described by two angles: the tilt angle τ, defined as the angle between the long axis of the helix and the membrane normal, and the azimuthal rotation angle ρ, which defines the rotation of the peptide around its long axis (see **Figure S1**). Using ^{2}H-NMR data from Ala-d_3 labeled positions, the helix orientation is calculated from RMSD fits and quadrupolar wave plots, as described previously (6-8).

To calculate orientational constraints from the NMR data, a quadrupolar coupling constant (e^2qQ/h) of 167 kHz for an aliphatic C-D bond was used, giving a maximum quadrupole splitting of 84 kHz for the CD_3-groups of the Ala-d_3 labels (9). The quadrupole splitting $\Delta\nu_q$ is then given by

$$\Delta\nu_q = 84 \text{ kHz} \times \tfrac{1}{2}\langle 3\cos^2\theta - 1\rangle \qquad (1)$$

where ⟨ ⟩ represents the time average, and θ is the angle between the C-CD_3 bond and the external magnetic field B_0.

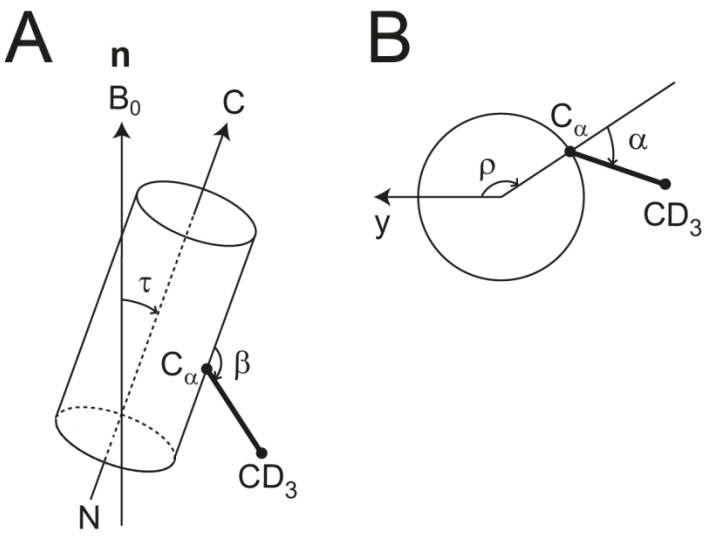

Figure S1. Definition of angles used in this work. (A) The helix tilt angle τ is the angle between the peptide axis (from N- to C-terminus) and the bilayer normal **n** (which in NMR experiments is usually aligned parallel to the magnetic field direction B_0). For τ = 0°, the helix would be oriented along **n**. The angle β fixes the C_α-CD_3 bond vector relative to the helix axis. (B) View perpendicular to the helix axis, with the C-terminus pointing out of the paper plane. The azimuthal rotation of the peptide is defined by the angle ρ. We define ρ = 0° such that the radial vector from the helix center through the C_α atom of residue 12 is aligned with the y-axis, which is parallel to the membrane surface. The projection of the C_α-CD_3 bond vector onto the plane perpendicular to the helix axis is fixed by the angle α.

For the NMR analysis, the structure of MAG2 was modeled as an ideal α-helix, and the alignment of this helix was fitted to the orientational constraints. In the molecular frame, the tilt angle τ defines the angle between the helix axis (defined from the N- to the C-terminus) and the bilayer normal. The azimuthal angle ρ is defined as a right-handed rotation around the helix axis, where ρ = 0° means that a radial vector from the helix axis to the C_α-atom of Phe-12 is oriented parallel to the membrane surface (6,10). The orientation of the C_α-C_β bond in the molecular frame is described by an angle β between the bond vector and the helix axis, and an angle α, defined by the vector radiating from the helix axis through the C_α-atom and by the projection of the C_α-C_β bond vector onto a plane perpendicular to the helix. In the same plane, the rotational angle between two consecutive amino acids along the helix is called ω. The angles are explained

in **Figure S1**. We described an α-helix using a β of 121.1°, an α of 53.2°, and an ω of 100°, as determined from an α-helical polyalanine model constructed in SYBYL (Tripos, St. Louis, USA) using the torsion angles φ = -58° and ψ = -47° (10).

Peptide dynamics are described in terms of whole-body fluctuations by Gaussian distributions of the τ and ρ angles, with widths given by the standard deviations σ_τ and σ_ρ, respectively. Larger widths correspond to a more dynamic situation, in which the angles undergo more vigorous fluctuations with larger amplitudes. It is justified to assume that these fluctuations are fast on the NMR time scale, so that the measured splittings represent time-averages over these distributions (11,12). In a grid search for the best-fit peptide structure, the helix is systematically rotated, and the theoretical quadrupole splittings are calculated for different combinations of τ, ρ, σ_τ and σ_ρ. All parameters are changed in steps of 1°; τ and ρ are investigated over the range from 0 to 180°, and σ_τ and σ_ρ from 0 to 50°, which was found to be a large enough range of dynamics to cover the point with the lowest root-mean-square deviation (RMSD) with respect to the experimental data. This way, we identified the best-fit parameters τ, ρ, σ_τ and $\sigma_{\rho,}$ which describe the orientation and dynamics of the peptide.

Molecular dynamics simulations

Simulation setup and parameters. Simulations were conducted for a single MAG2 in a DMPC bilayer consisting of 128 lipids solvated with 5700 TIP3P water molecules (13) and neutralized with chloride ions, and in a DMPC/DMPG bilayer with 96 DMPC and 32 DMPG lipids with 7000 water molecules and neutralized with sodium ions. The SLIPID force field was used for the lipids (14), and the AMBER99SB-ILDN (15) force field for everything else. This parameter combination has been used earlier, where it was shown that experimental parameters are well reproduced (16). The peptides were initially modeled as ideal α-helices using the *xleap* tool from the AmberTools modeling suite, using backbone torsion angles of φ = -57° and ψ= -47° (17). Simulations were performed with the GROMACS simulation package version 4.5.5 (simulation in DMPC) and 4.6.3 (simulation in DMPC/DMPG). The peptide-membrane complexes were constructed by conducting unrestrained membrane binding simulations of 10 ns duration, by placing the peptide molecules parallel to pre-equilibrated lipid bilayers at a distance of 2.5 nm, at an elevated temperature of 480 K to speed up insertion (using a simulation protocol from (18)). During the high-temperature insertion, hydrogen bonds in the helical peptides were restrained using distance restraints of 1000 kJ/(mol nm^2) to prevent unfolding. After cooling down to 303

K, a short equilibration run of 500 ps with position restraints of 1000 kJ/(mol nm^2) on the membrane-bound peptides was performed to allow temperature and volume to stabilize. Then, the systems were simulated for one microsecond in DMPC, and 700 ns in DMPC/DMPG, without any restraints at 303 K in the NPT ensemble, with snapshots saved every 50 ps. This unrestrained production simulation was conducted using a Nosé-Hover thermostat (19) and Parrinello-Rahman barostat at 1 bar (20) with semi-isotropic pressure coupling. A time step of 2 fs was used for all simulations, together with the LINCS algorithm (21) to constrain all bonds. Long-range electrostatics were treated via particle-mesh Ewald (22), combined with a 1.4 nm direct space cut-off for van der Waals and Coulomb interactions.

Peptide orientation. The orientation of the peptide was first determined independently by calculating τ and ρ directly from the simulation. From each simulation snapshot (taken every 50 ps) the τ and ρ angles were extracted and the average over all snapshots was calculated. The helix axis is defined for each snapshot as a vector pointing from the center of mass of the N-terminal half of the peptide to the center of mass of the C-terminal half of the peptide, taking into account only heavy backbone atoms in the helical part of the peptide, positions 3-16. The τ angle is calculated as the angle between this vector and the z-axis. The ρ angle is defined from an average position of the C_α-atoms for all residues in the helical part of the peptide, shifted to position 12 (by a shift of 100° per residue for an ideal α-helix). The error on ρ for each time step has been calculated as $\varepsilon_\rho(t) = \sqrt{1/(14 \cdot 13) \sum_{i=3}^{16} \left[\langle \rho(t) \rangle_{i \in [3;16]} - \rho_i(t)\right]^2}$.

To determine which initial part of the simulation should be discarded due to equilibration, an error analysis was performed, using the GROMACS tool *g_analyze.* The tool uses block averaging to estimate the error on the average of the time series of an observable, taking into account the correlation between chronologically close snapshots (23). The error was repeatedly calculated, while discarding different initial parts of the simulation between 10 and 200 ns. The final statistical analysis was done by discarding the initial interval which yielded the minimal sum of the errors for τ and ρ (see **Figure S2**). For DMPC the first 140 ns were discarded, and in the DMPC/DMPG simulation the first 160 ns were discarded.

Table S2. ^{2}H-NMR splittings (in kHz) back-calculated from the MD trajectory.

	DMPC			**DMPC/DMPG**		
Position	$\Delta\nu_q$	ε^a	**SD**[b]	$\Delta\nu_q$	ε^a	**SD**[b]
Gly-1	-11.8	2.5	35.3	-14.3	4.6	31.1
Ile-2	40.2	2.4	23.9	25.5	2.3	21.7
Gly-3	15.9	10.0	23.6	31.2	3.9	23.0
Lys-4	-7.3	3.2	23.3	-0.9	3.9	23.9
Phe-5	24.9	3.1	21.0	7.9	3.2	20.1
Leu-6	-30.8	2.4	13.2	-35.2	1.5	9.4
His-7	45.9	(12.3)	16.9	62.9	2.4	13.8
Ser-8	-34.8	0.7	9.2	-37.0	0.4	6.8
Ala-9	29.4	7.6	19.3	8.7	4.0	19.4
Leu-10	-15.9	9.0	18.0	-3.4	6.3	21.8
Leu-11	13.9	3.9	23.8	26.6	3.7	23.4
Phe-12	9.7	2.4	20.7	-7.0	3.5	20.7
Gly-13	-26.2	3.1	16.0	-33.0	2.0	11.7
Lys-14	31.5	11.7	21.8	56.9	5.0	19.5
Ala-15	-26.0	2.7	17.1	-28.6	2.9	15.9
Phe-16	33.5	(16.0)	20.7	25.6	4.9	21.3
Val-17	22.6	(43.8)	40.2	-31.8	3.6	14.1
Gly-18	-17.6	5.5	19.1	-7.9	6.5	25.0
Glu-19	-8.7	19.5	27.6	-24.9	(20.1)	19.2
Ile-20	38.6	(19.5)	27.6	50.5	5.8	25.7
Met-21	19.3	4.7	31.9	-6.3	11.8	33.7
Asn-22	-26.8	3.2	19.2	-25.2	10.2	18.6
Ser-23	-18.7	6.6	24.4	-1.6	8.2	35.6

[a] Error estimate from a block analysis using *g_analyze* (23). Brackets indicate that a fit was only possible by setting the fitting parameter τ_2 to either the total evaluated simulation length or to zero; i.e. insufficient statistics.

[b] Standard deviation of splittings over all snapshots of the simulation (discarding initial equilibration).

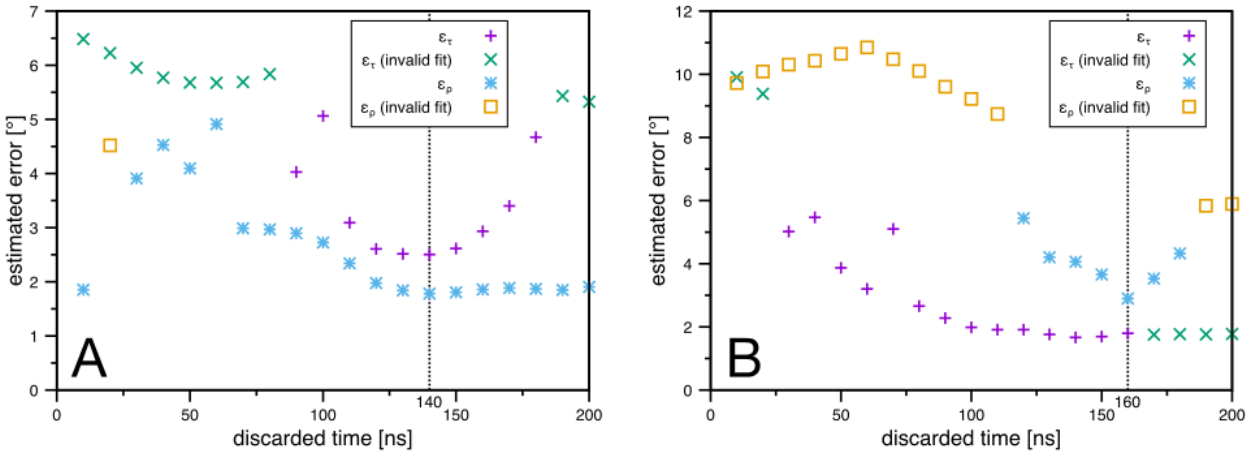

Figure S2. Estimated error for different discarded initial parts of the simulation, estimated with *g_analyze* (23). Data "invalid fit" indicate that a fit was only possible by setting the fitting parameter τ_2 to either the total evaluated simulation length or to zero; i.e. insufficient statistics. (A) MAG2 in DMPC, total simulation length 1 μs. The minimum of $\varepsilon_\tau + \varepsilon_\rho$ is at 140 ns. (B) MAG2 in DMPC/DMPG (3:1), total length 700 ns. The minimum of $\varepsilon_\tau + \varepsilon_\rho$ is at 160 ns.

The distributions of τ and ρ over the remaining part of the simulations (140-1000 ns in DMPC; and 160-700 ns in DMPC/DMPG (3:1)) were fitted to a Gaussian function to determine the standard deviations σ_τ and σ_ρ.

Hypothetical ^{2}H quadrupole splittings were then back-calculated from the orientation of the relevant C_α-C_β bonds of the native amino acids with respect to the membrane normal (the z-axis in the simulation box), which corresponds to the orientation of the external magnetic field in the NMR experiments. In the case of Gly residues, where no C_β atom is present, the corresponding C_α-H_α bond was used (i.e., as if the Gly residue was replaced by *L*-Ala). The quadrupole splittings were obtained from the simulations by calculating the bond order parameter $S_{CD}=½\langle 3\cos^2\theta - 1\rangle$, where θ is the angle between the C_α-C_β bond of the residue under consideration and the membrane normal, and multiplying this value with 84 kHz. The initial parts of the simulations, 140 ns for the DMPC system and 160 ns for DMPC/DMPG (3:1), were discarded to be consistent with the values for τ and ρ obtained directly, and the splittings were averaged over the rest of the simulation. The results are given in **Table S2**. The error on the splittings was calculated with *g_analyze* as mentioned above and as explained in (23).

To compare the NMR and MD results, the simulated ^{2}H-splittings were compared with the experimental ones, and the simulated ^{2}H-splittings were analyzed in the same way as the experimental splittings to determine the peptide orientation according to these splittings.

Peptide helicity. The helicity of the peptide in the simulations was determined for each residue based on the dihedral angles φ and ψ. If both of these angles are within 30° from the standard values for an α-helix, defined as φ = -57° and ψ = -47°, the residue is considered to be in a helical configuration, and the percentage helix is given by the number of time steps in which this condition is fulfilled, divided by the total number of time steps. This means that a residue is considered to be 100% helical if the condition is fulfilled for all evaluated time steps (140-1000 ns in DMPC, 160-700 ns in DMPC/DMPG).

Interaction analysis. The average position of the phosphorus atoms was calculated by averaging over the z-coordinate of the phosphorus of all lipids in the upper leaflet, but discarding snapshots where the peptide's center of mass was closer than 2 nm to the phosphorus atom, to ignore the influence of the peptide on the position of the lipid head groups. The error on the average was obtained by calculating average values for each lipid and then calculating the statistical error from these averages:

$$\varepsilon_{Pz} = \sqrt{1/(N(N-1))\sum_{i=1}^{N}\left[\langle P_{z,all}\rangle - \langle P_{z,i}\rangle\right]^2}.$$

The error on the z-coordinate of the oxygens of Glu-19, Ser-23 and MAG2 was estimated using *g_analyze*. The values and errors are given in **Table S3**. The average membrane center was determined by averaging the values obtained for the undisturbed phosphorus of the upper leaflet and all phosphorus of the lower leaflet.

Table S3. Average z coordinates with respect to the membrane center. Brackets indicate that a fit was only possible by setting the fitting parameter τ_2 to either the total evaluated simulation length or to zero; i.e. insufficient statistics.

	Δz to membrane center (nm)	Error (nm)
DMPC		
P upper leaflet, excluding lipids within 2 nm of peptide	1.70	0.01
MAG2 (center of mass)	1.20	0.09
Glu-19, O1	1.71	(0.22)
Glu-19, O2	1.71	(0.22)
Ser-23, O1	1.92	(0.17)
Ser-23, O2	1.92	(0.16)
DMPC/DMPG (3:1)		
P upper leaflet, excluding lipids within 2 nm of peptide	1.79	0.01
MAG2 (center of mass)	1.06	
Glu-19, O1	1.46	0.05
Glu-19, O2	1.48	(0.04)
Ser-23, O1	1.82	0.07
Ser-23, O2	1.81	0.07

^{2}H-NMR SPLITTINGS

The splittings were determined from the NMR spectra. In all cases a central peak was observed, which is due in part to residual ^{2}H nuclei in water and can be observed also in samples without peptide. The ^{2}H-NMR signals from peptides in the oriented membranes give two symmetrical peaks with a splitting dependent on the orientation of the C-CD_3 bond. Spectra are shown in **Figure 2** in the main text, but are also included here in **Figures S3 and S4** enlarged and scaled to better show the signals and indicate the splittings.

In POPC/POPG samples, splittings are usually clearly visible. They are shown in red in **Figure S3A**. In MAG-F12A no splitting is seen, probably because it happens to be too small to be resolved form the central peak. It is assumed that the splitting in this case is 0 kHz. This value fits the helical curve obtained from a fit to the other data points, supporting this interpretation (**Figure 4C**). There are some additional splittings with low intensity visible in the spectra (marked in blue). In MAG2-F12A, there is a shoulder on the main peak, with a possible splitting of around 8 kHz, but the intensity is very low. In MAG2-V17A, a splitting of approximately 38 kHz is seen. This is a value typically found for aggregated peptides (24), and can therefore be due to some immobilized peptide fraction. In MAG2-I20A there is a smaller splitting seen, 14.1 kHz, which is very close to half the main splitting. This is most likely a signal from peptides in unoriented vesicles, where fast rotation around the bilayer normal will give a splitting averaged by a factor of ½ (7).

In DMPC/DMPG at P/L=1:100, clear splittings are seen in all cases, marked in red in **Figure S3B**. In MAG2-F5A there is also a smaller intensity splitting (marked in blue), which equals half the main splitting, most likely also due to unoriented parts of the sample.

In DMPC/DMPG at P/L=1:50 (**Figure S4A**), splittings are harder to define. In MAG2-F5A, -F12A, and -G18A, only a central peak is found. In the other cases, splittings are seen (marked in red), but are sometimes not as clear as in DMPC/DMPG at P/L=1:100. Even though the amount of peptide per sample is the same in both cases, the intensity of the ^{2}H-NMR signal from the peptide is lower at the higher concentration for some unknown reason. It could have something to do with a change in mobility which can affect relaxation behavior. In MAG2-V17A, there are two possible splittings with similar intensities. The smaller splitting is 29.9 kHz. The larger splitting (marked in blue) is 36.8 kHz, close to the powder splitting, and therefore somewhat suspicious since it could be due to immobilized peptides. In MAG2-I20A there are

also two possible splittings. The smaller one (7.9 kHz) has a higher intensity, which might be because it is close to the central peak and overlaps with the flanks of the central peak. The larger one (13.5 kHz) is slightly asymmetric around the central peak. Since also here the smaller splitting is close to ½ of the larger one, it may be due to signals from unoriented parts of the sample (like for MAG2-F5A in DMPC/DMPG P/L=1:50). We can note that the clearest splittings (from MAG2-L6A, -A9, -G13A, -A15 and -F16A) are not very different from the splittings at the same position in DMPC/DMPG P/L=1:100 (within 5 kHz). This indicates that the peptide orientation is not changing much, and makes it likely that also the other splittings should be quite similar. This would make it more likely that the splitting of MAG2-V17A is 29.9 kHz rather than the larger splitting of 36.8 kHz also seen, and that the splitting of MAG2-I20A is 13.5 kHz rather than 7.9 kHz. The similarity of splittings at 1:100 and 1:50 also makes it reasonable to assume that the splitting of MAG2-F12A can be close to 0 kHz, but this assumption cannot be made for MAG2-F5A and MAG2-G18A, where large splittings were observed in DMPC/DMPG P/L=1:100. Therefore the spectra of MAG2-F5A and MAG2-G18A are not assigned a splitting and are not included in the analysis.

Several fits were made using different combinations of data in DMPC/DMPG P/L=1:50, as shown in **Figure S5** and **Table S4**. For position 18, 29.9 kHz or 36.8 kHz were used, and for position 20, either 13.5 kHz or 7.9 kHz. In all cases, a very similar best fit was found, within 1° of the fit shown in the main text, with tau = 94° and rho = 174° (**Figure S3, A-C**). Also when positions 18, 20, or both were not used at all in the fit, the same result was found (**Figure S3, D-F**), so the exact splittings of these positions were not critical for the result.

Finally, in DMPC/DMPG (**Figure S4B**) with PGLa, no clear splittings are seen in MAG2-F5A, -A9 and -F12A. In the other samples, clear splittings are seen (marked in red). These splittings are sometimes very different from the splittings found in DMPC/DMPG without PGLa (up to 30 kHz changes in the absolute values), and therefore it is not possible to assume anything about the spectra without clear splittings. It is possible that those splittings are really zero, but it could also be a problem with signal intensities. Therefore those positions were not assigned a splitting and are not used in the data analysis.

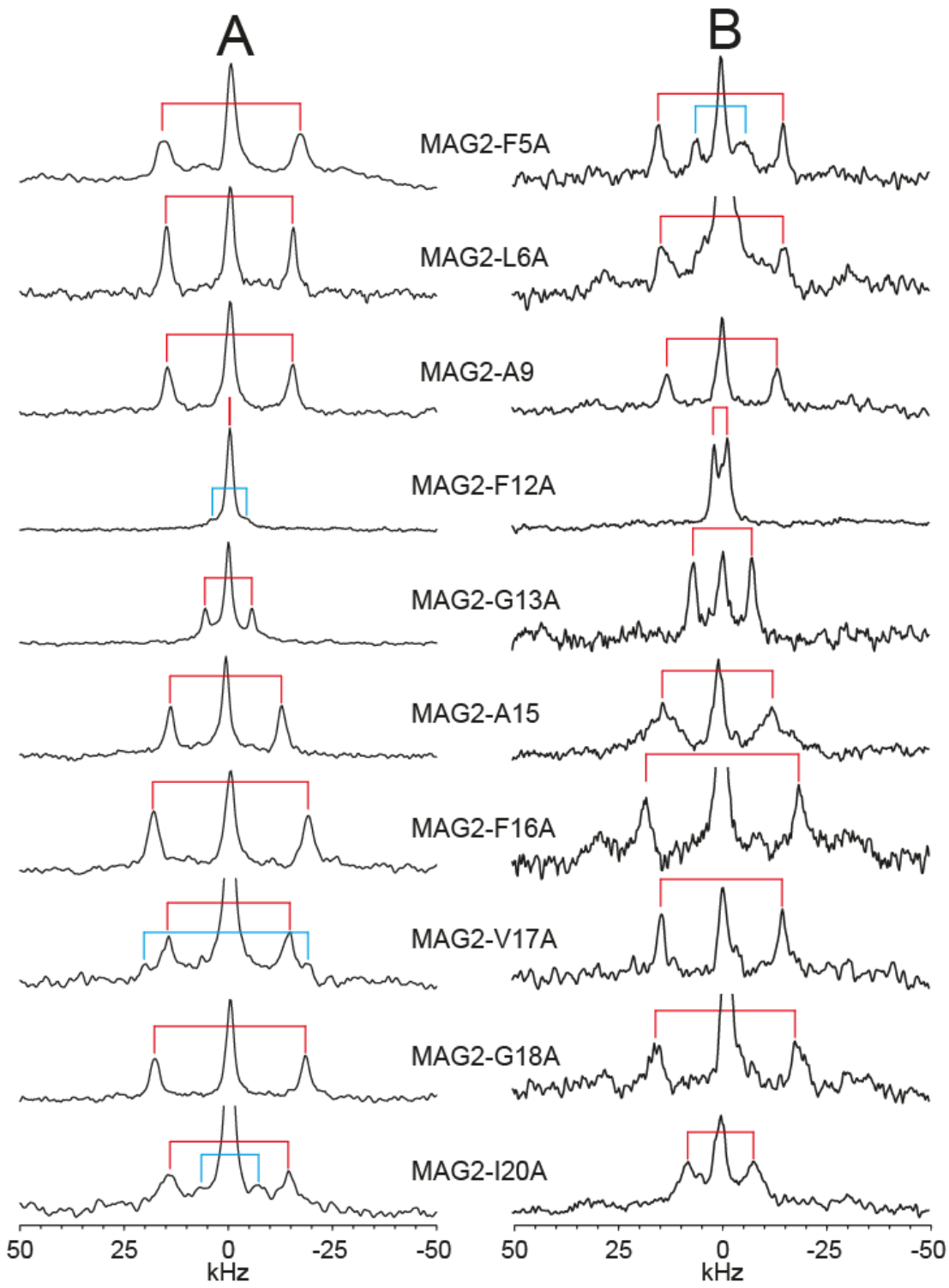

Figure S3. Splittings found in ^{2}H-NMR spectra. (A) MAG2 in POPC/POPG (9:1). (B) MAG2 in DMPC/DMPG (3:1), P/L=1:100. Main splittings are marked in red, minor splittings in blue. All samples were prepared using method 1.

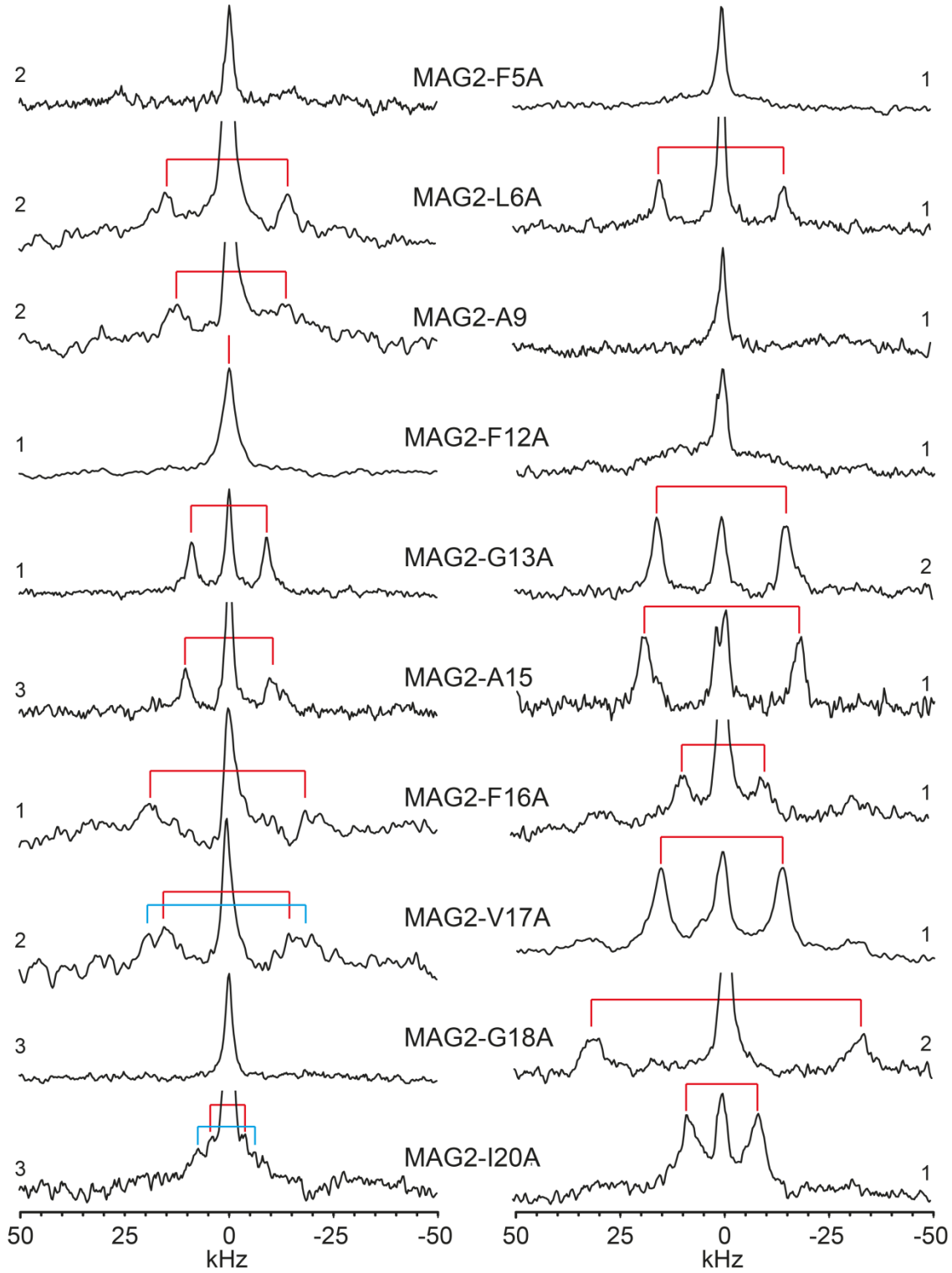

Figure S4. Splittings found in ^{2}H-NMR spectra. (A) MAG2 in DMPC/DMPG (3:1). P/L=1:50. (B) MAG2 with PGLa in DMPC/DMPG (3:1), P/P/L=1:1:100. Main splittings are marked in red, minor splittings in blue. Numbers next to each spectrum indicate the sample preparation method used.

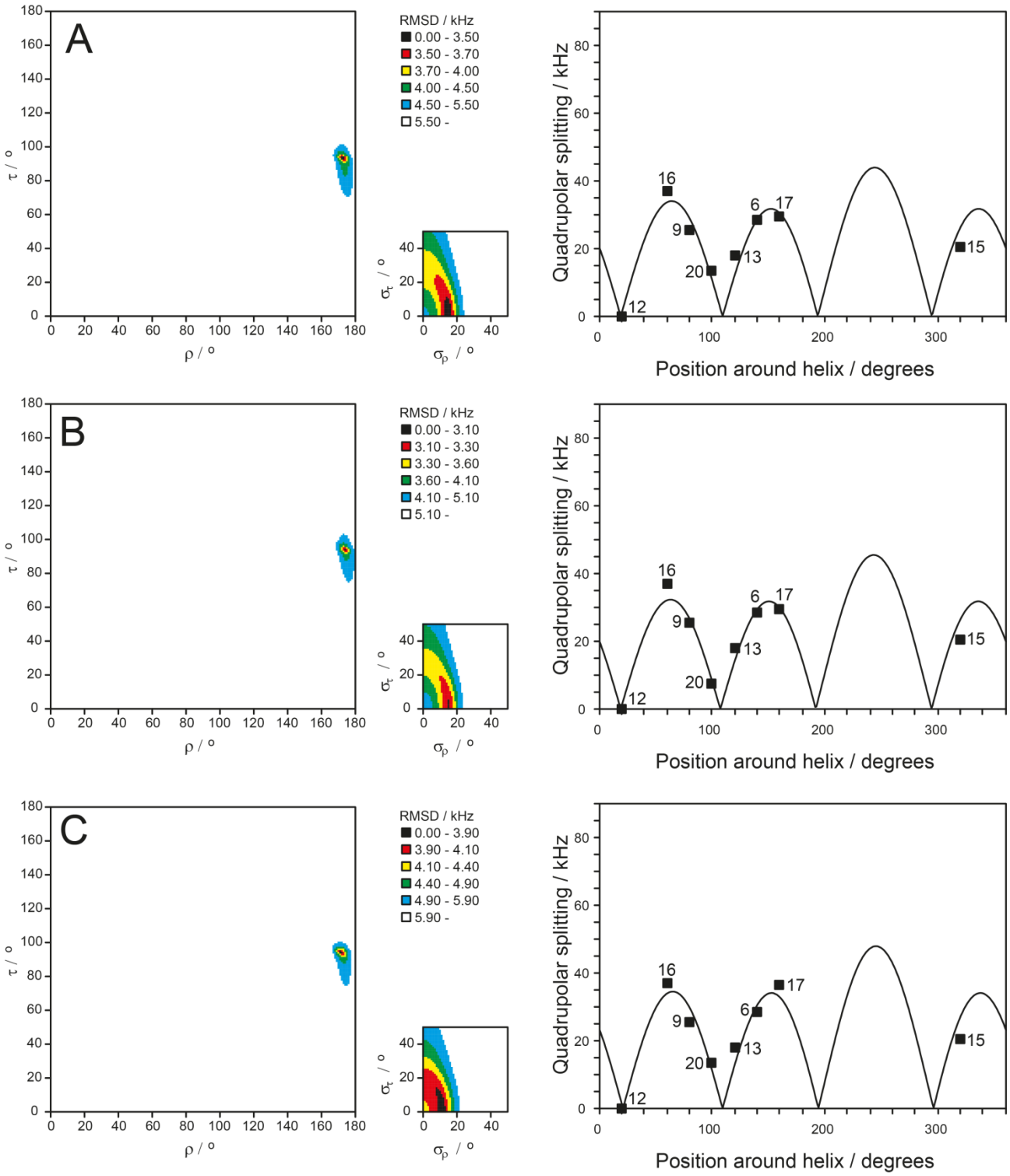

Figure S5. Fits of various data sets for MAG2 in DMPC/DMPG (3:1). P/L=1:50. (A) Fit using values from Table 1 in the main text. (B) Like (A), but using for position 20 a splitting of 7.9 kHz. (C) Like (A), but using for position 17 a splitting of 36.8 kHz.

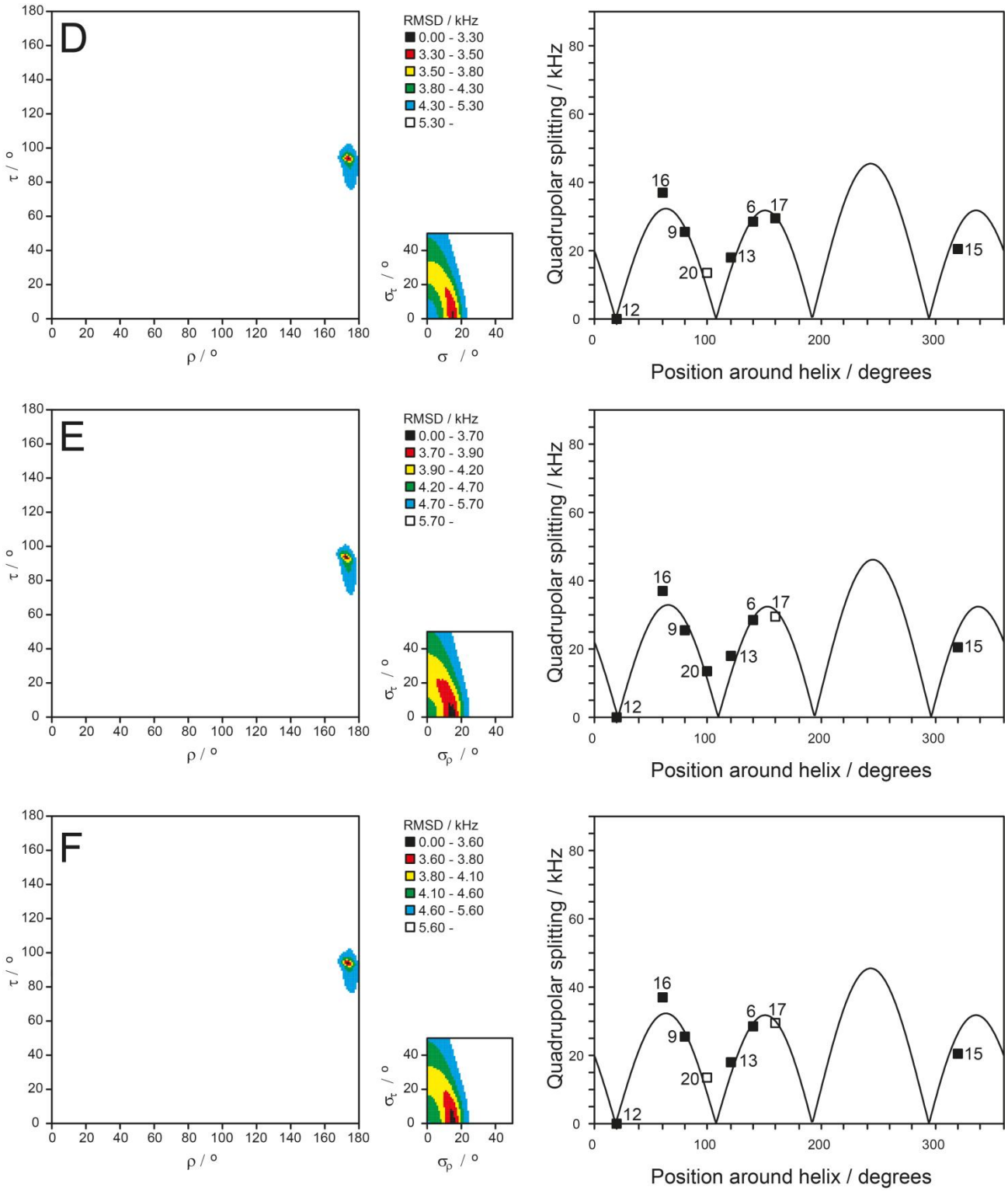

Figure S5 (continued). Fits of various data sets for MAG2 in DMPC/DMPG (3:1). P/L=1:50. (D) Fit not using data from position 20. (E) Fit not using data from position 18. (F) Fit not using data from position 18 and 20.

Table S4. Fits of MAG2 in DMPC/DMPG P/L=1:50, using different ^{2}H-NMR data sets.

Method	Lipid system	P/L	Positions used in fit	τ (°)	ρ (°)	σ_τ (°)	σ_ρ (°)	RMSD (kHz)
^{2}H-NMR	DMPC/DMPG	2:75:25	8 [a]	93	173	1	15	3.4
	DMPC/DMPG	2:75:25	8 [b]	94	174	1	15	3.1
	DMPC/DMPG	2:75:25	8 [c]	94	172	0	11	3.8
	DMPC/DMPG	2:75:25	7 [d]	94	174	1	15	3.3
	DMPC/DMPG	2:75:25	7 [e]	94	174	1	15	3.3
	DMPC/DMPG	2:75:25	6 [f]	94	174	1	15	3.5

[a] 5, 18 not used. 17 = 29.9 kHz, 20 = 13.5 kHz.

[b] 5, 18 not used. 17 = 29.9 kHz, 20 = 7.6 kHz.

[c] 5, 18 not used. 17 = 36.8 kHz, 20 = 13.5 kHz.

[d] 5, 17, 20 not used.

[e] 5, 17, 18 not used.

[f] 5, 17, 18, 20 not used.

HELICAL WHEELS OF MAGAININ 2 AND PGLA IN MEMBRANES

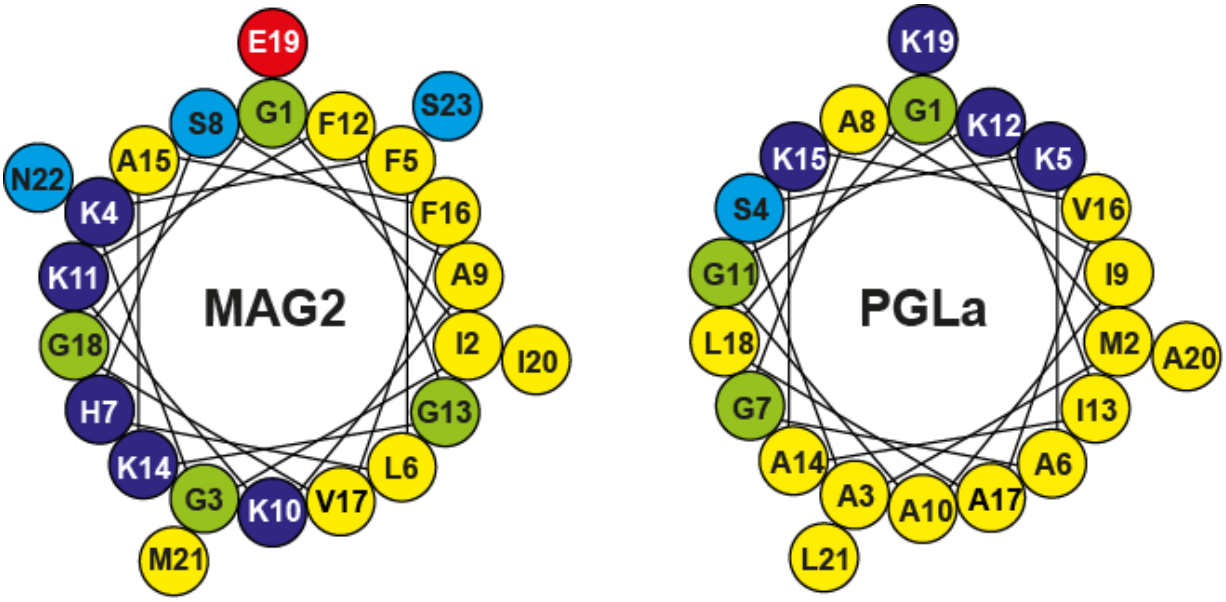

Figure S6. Helical wheels of MAG2 and PGLa. Hydrophobic residues are marked in yellow, polar in light blue, cationic in dark blue, anionic in red, glycines in green.

ORIENTATION OF MAGAININ 2 IN MEMBRANES

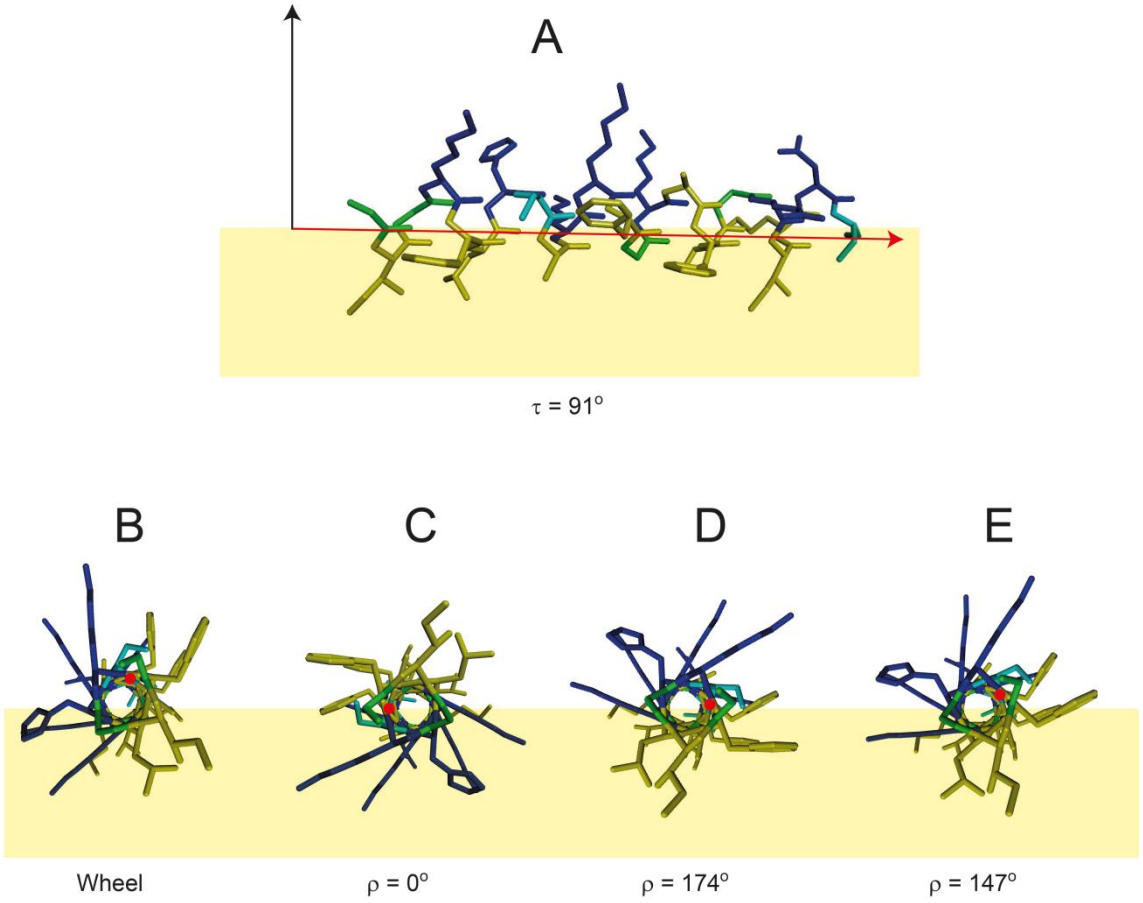

Figure S7. Illustration of the orientation of MAG2 in membranes according to a fit of ^{2}H-NMR data. The peptide is seen along the axis in a stick representation, where hydrophobic residues are yellow, Lys and His dark blue, Glu light blue and Gly green. The hydrophobic part of the membrane is shown as a yellow box (thickness not in scale). (A) MAG2 seen from the side in the membrane. The tilt angle (τ) of 91° means that the helix axis (red arrow), from N- to C-terminal, is rotated 91° from the membrane normal (black arrow). The C-terminus is inserted slightly deeper into the membrane than the N-terminus. (B-E) MAG2 seen along the helix axis, with the C-terminus in front, flat on the membrane. The red dot shows the position of C_α of the reference residue Phe-12. (B) Orientation as in the helical wheel in **Figure S6**. C_α of position 1 points up. (C) Reference orientation where the azimuthal angle ρ is set to 0°. In this case, a vector from the helix axis to C_α of Phe-12 lies in the plane of the membrane. (D) The orientation found for MAG2 alone in POPC/POPG or DMPC/DMPG lipids, with ρ = 174°. All charged residues point out of the membrane. (E) The orientation found for MAG2 together with PGLa in DMPC/DMPG lipids, with ρ = 147°. In this case, C_α of Lys-10 is deeper in the membrane, and C_α of Glu-21 is pointing more to the water. The charged residues can snorkel so that the charges are outside the membrane even if C_α is deeper down. It should also be noted that the depth of membrane insertion is not known from the NMR data, here in all cases the helix axis is shown to be in the plane of the membrane.

SUPPORTING REFERENCES

1. Fields, G. B., and R. L. Noble. 1990. Solid-phase peptide synthesis utilizing 9-fluorenylmethoxycarbonyl amino acids, *Int. J. Pept. Protein Res.* 35:161-214.
2. Strandberg, E., J. Zerweck, D. Horn, G. Pritz, P. Wadhwani, M. Berditsch, J. Bürck, and A. S. Ulrich. 2015. Influence of hydrophobic residues on the activity of the antimicrobial peptide magainin 2 and its synergy with PGLa, *J. Pept. Sci.* 21:436-445.
3. Rance, M., and R. A. Byrd. 1983. Obtaining high-fidelity spin-1/2 powder spectra in anisotropic media - phase-cycled Hahn echo spectroscopy, *J. Magn. Reson.* 52:221-240.
4. Davis, J. H., K. R. Jeffrey, M. Bloom, M. I. Valic, and T. P. Higgs. 1976. Quadrupolar echo deuteron magnetic resonance spectroscopy in ordered hydrocarbon chains, *Chem. Phys. Lett.* 42:390-394.
5. Strandberg, E., N. Kanithasen, J. Bürck, P. Wadhwani, D. Tiltak, O. Zwernemann, and A. S. Ulrich. 2008. Solid state NMR analysis comparing the designer-made antibiotic MSI-103 with its parent peptide PGLa in lipid bilayers, *Biochemistry*. 47:2601-2616.
6. Glaser, R. W., C. Sachse, U. H. N. Dürr, S. Afonin, P. Wadhwani, E. Strandberg, and A. S. Ulrich. 2005. Concentration-dependent realignment of the antimicrobial peptide PGLa in lipid membranes observed by solid-state ^{19}F-NMR, *Biophys. J.* 88:3392-3397.
7. Strandberg, E., S. Özdirekcan, D. T. S. Rijkers, P. C. A. Van der Wel, R. E. Koeppe, II, R. M. J. Liskamp, and J. A. Killian. 2004. Tilt angles of transmembrane model peptides in oriented and non-oriented lipid bilayers as determined by ^{2}H solid state NMR, *Biophys. J.* 86:3709-3721.
8. Strandberg, E., P. Wadhwani, P. Tremouilhac, U. H. N. Dürr, and A. S. Ulrich. 2006. Solid-state NMR analysis of the PGLa peptide orientation in DMPC bilayers: structural fidelity of ^{2}H-labels versus high sensitivity of ^{19}F-NMR, *Biophys. J.* 90:1676-1686.
9. Davis, J. H. 1983. The description of membrane lipid conformation, order and dynamics by ^{2}H-NMR, *Biochim. Biophys. Acta*. 737:117-171.
10. Glaser, R. W., C. Sachse, U. H. N. Dürr, P. Wadhwani, and A. S. Ulrich. 2004. Orientation of the antimicrobial peptide PGLa in lipid membranes determined from ^{19}F-NMR dipolar couplings of 4-CF_3-phenylglycine labels, *J. Magn. Reson.* 168:153-163.
11. Strandberg, E., S. Esteban-Martín, J. Salgado, and A. S. Ulrich. 2009. Orientation and dynamics of peptides in membranes calculated from ^{2}H-NMR data, *Biophys. J.* 96:3223-3232.
12. Strandberg, E., and A. S. Ulrich. 2014 Dynamic structure analysis of peptides in membranes by solid-state NMR, *In* Advances in Biological Solid-State NMR: Proteins and Membrane-Active Peptides. F. Separovic, and A. Naito, editors. Royal Society of Chemistry, London, pp. 304-319.
13. Jorgensen, W. L., J. Chandrasekhar, J. D. Madura, R. W. Impey, and M. L. Klein. 1983. Comparison of simple potential functions for simulating liquid water, *J. Chem. Phys.* 79:926-935.
14. Jämbeck, J. P., and A. P. Lyubartsev. 2012. Derivation and systematic validation of a refined all-atom force field for phosphatidylcholine lipids, *J. Phys. Chem. B.* 116:3164-3179.
15. Lindorff-Larsen, K., S. Piana, K. Palmo, P. Maragakis, J. L. Klepeis, R. O. Dror, and D. E. Shaw. 2010. Improved side-chain torsion potentials for the Amber ff99SB protein force field, *Proteins*. 78:1950-1958.

16. Reißer, S. 2014. Computational studies of membrane-active antimicrobial peptides and comparison with NMR data. PhD thesis. Karlsruhe Institute of Technology, Karlsruhe.
17. Case, D. A., T. A. Darden, …, P. A. Kollman 2012 *AMBER 12*, University of California, San Francisco.
18. Ulmschneider, J. P., J. C. Smith, M. B. Ulmschneider, A. S. Ulrich, and E. Strandberg. 2012. Reorientation and dimerization of the membrane-bound antimicrobial peptide PGLa from microsecond all-atom MD simulations, *Biophys. J.* 103:472-482.
19. Nosé, S. 1984. A molecular dynamics method for simulations in the canonical ensemble, *Mol. Phys.* 52:255-268.
20. Parrinello, M., and A. Rahman. 1981. Polymorphic transitions in single crystals - a new molecular dynamics method, *J. Appl. Phys.* 52:7182-7190.
21. Hess, B., H. Bekker, H. J. C. Berendsen, and J. G. E. M. Fraaije. 1997. LINCS: A linear constraint solver for molecular simulations, *J. Comp. Chem.* 18:1463-1472.
22. Darden, T., D. York, and L. Pedersen. 1993. Particle mesh Ewald - an $N \bullet \log(N)$ method for Ewald sums in large systems, *J. Chem. Phys.* 98:10089-10092.
23. Hess, B. 2002. Determining the shear viscosity of model liquids from molecular dynamics simulations, *J. Chem. Phys.* 116:209-217.
24. Strandberg, E., D. Tiltak, S. Ehni, P. Wadhwani, and A. S. Ulrich. 2012. Lipid shape is a key factor for membrane interactions of amphipathic helical peptides, *Biochim. Biophys. Acta*. 1818:1764-1776.